

Stellar Binaries That Survive Supernovae

C. S. Kochanek^{1,2}, K. Auchettl³ and C. Belczynski⁴

¹ *Department of Astronomy, The Ohio State University, 140 West 18th Avenue, Columbus OH 43210*

² *Center for Cosmology and AstroParticle Physics, The Ohio State University, 191 W. Woodruff Avenue, Columbus OH 43210*

³ *Dark Cosmology Centre, Niels Bohr Institute, University of Copenhagen, Juliane Maries Vej 30, 2100, Copenhagen, Denmark*

⁴ *Nicolaus Copernicus Astronomical Center, Polish Academy of Sciences, ul. Bartycka 18, 00-716 Warsaw, Poland*

23 October 2018

ABSTRACT

The number of binaries containing black holes (BH) or neutron stars (NS) depends critically on the fraction of binaries that survive supernova (SN) explosions. We searched for surviving star plus remnant binaries in a sample of 49 supernova remnants (SNR) containing 23 previously identified compact remnants and three high mass X-ray binaries (HMXB), finding no new interacting or non-interacting binaries. The upper limits on any main sequence stellar companion are typically $\lesssim 0.2M_{\odot}$ and are at worst $\lesssim 3M_{\odot}$. This implies that $f < 0.1$ of core collapse SNRs contain a non-interacting binary, and $f = 0.083$ ($0.032 < f < 0.17$) contain an interacting binary at 90% confidence. We also find that the transverse velocities of HMXBs are low, with a median of only 12 km/s for field HMXBs, so surviving binaries will generally be found very close to the explosion center. We compare the results to a “standard” **StarTrack** binary population synthesis (BPS) model, finding reasonable agreement with the observations. In particular, the BPS models predict that 5% of SNe should leave a star plus remnant binary.

Key words: stars: massive – supernovae: general – supernovae

1 INTRODUCTION

Most massive stars are in binaries (see, e.g., Sana et al. 2012, Duchêne & Kraus 2013, Kobulnicky et al. 2014 and Moe & Di Stefano 2017). For example, Moe & Di Stefano (2017) find that only $16 \pm 8\%$ of stars that dominate the core-collapse supernova (ccSN) rate are single. Binary evolution, through mass transfer, mass loss, and merging, modifies the binary population as the stars evolve (e.g., Eldridge et al. 2008, Sana et al. 2012, Renzo et al. 2018, Zapartas et al. 2017). Then, when the primary explodes, the binary can become unbound either due to mass loss (Blaauw 1961) or “kicks” due to the explosion (e.g., Gunn & Ostriker 1970, Iben & Tutukov 1996, Cordes & Chernoff 1998, Faucher-Giguère & Kaspi 2006). For the binaries which survive, further evolution can lead to high and low mass X-ray binaries (HMXBs and LMXBs, see, e.g., the reviews by Remillard & McClintock 2006, Reig 2011, or Walter et al. 2015), and the explosion (or collapse) of the secondary can lead to the formation of neutron star (NS) and black hole (BH) binaries that can be gravitational wave sources (e.g., Abbott et al. 2016, Abbott et al. 2017). This means that the fraction of binaries which survive ccSNe and their properties are crucial ingredients for any process involving NS or BH binaries.

A simple toy model assuming passively evolving binaries (i.e., no interactions) can help frame the basic statis-

tics (Kochanek 2009). We can view the effective binary fraction as $F = F_0(1 - f_m) \simeq 55\%$, where $F_0 \simeq 84\%$ (Moe & Di Stefano 2017) is the true initial binary fraction and f_m is the fraction of binaries which merge before a ccSN can occur. In our binary population synthesis (BPS) model (§2), we find $f_m = 34\%$, while Renzo et al. (2018) find $f_m \simeq 22^{+26}_{-9}\%$. The fractions of ccSNe which occur in stellar binaries, as a single stars (including merger remnants), and as explosions of a secondary (which may be in a binary with a compact remnant) are

$$f_b = \frac{F}{1 + Ff_q}, \quad f_1 = \frac{1 - F}{1 + Ff_q} \quad \text{and} \quad f_s = \frac{Ff_q}{1 + Ff_q}, \quad (1)$$

respectively, where $f_q = \int_0^1 q^{x-1} P(q) dq$, $x \simeq 2.35$ is the slope of a Salpeter (1955) initial mass function (IMF), $0 \leq q = M_2/M_1 \leq 1$ is the mass ratio and $P(q)$ with $\int_0^1 dq P(q) \equiv 1$ is the distribution of mass ratios. For constant $P(q)$ (see the discussions in Kobulnicky et al. 2014, Moe & Di Stefano 2017) from $q = 0$ to $q = 1$ for simplicity, the integral is $f_q = 0.426$. Given these assumptions, fraction $f_b \simeq 41\%$ to 57% of ccSNe occur in stellar binaries for effective binary fractions of $F = 50\%$ to 75% .

At the time of explosion, most stellar companions are relatively massive. If stars more massive than M_{SN} explode, then the fraction of companions above mass M_s in our simple model is $1 - (x - 1)M_s/xM_{SN} \simeq 1 -$

arXiv:1810.08620v1 [astro-ph.SR] 19 Oct 2018

$0.43M_s/M_{SN}$ for $M_s < M_{SN}$. If $M_{SN} = 8M_\odot$, 43% of stellar secondaries are massive enough to eventually explode, and 93%, 64% and 50% are more massive than $M_s > 1, 3$ and $5M_\odot$, respectively. Unlike searches for surviving single degenerate companions to Type Ia SNe (e.g., Schweizer & Middleditch 1980, Ruiz-Lapuente et al. 2004, Ihara et al. 2007, González Hernández et al. 2012, Schaefer & Pagnotta 2012), searches for stellar companions to ccSNe can focus on relatively high mass, luminous stars with only modest statistical penalties.

If we ignore kicks, the binary becomes unbound if the final system mass is less than one-half of the initial mass (Blaauw 1961). If the primary, secondary and neutron star (NS) remnant have masses of M_p , M_s and $M_{ns} \simeq 1.4M_\odot$, respectively, then the secondary must have $M_s > M_p - 2M_{ns}$ for the binary to survive. If the minimum mass for a ccSN is $M_{SN} \simeq 8M_\odot$, then only binaries with secondaries more massive than $M_s \gtrsim 5M_\odot$ can survive the formation of a NS. This means that in our non-interacting binary model, the fraction of binaries that survive the explosion of the primary is $2(x-1)M_{NS}/xM_{SN} \simeq 20\%$. For effective binary fractions of $F = 50\%$ to 75% , $\sim 10\%$ of core collapse SNRs should contain a star-NS binary and 30-45% of SNRs should contain a disrupted binary. The stars in disrupted binaries should, on average, be less massive than the ones still in binaries. These back of the envelope estimates come surprisingly close to the results of full population synthesis models. In §2 we find that 25% of stellar binaries survive the explosion in our BPS models, while Renzo et al. (2018) find that $14^{+22}_{-10}\%$ of binaries survive, but do not distinguish between companion types.

Searches for binary companions to ccSNe are largely restricted to the Galaxy and potentially the Magellanic Clouds. For ccSN in nearby (1-30 Mpc) galaxies, there are two problems. First, only the most luminous secondaries can be detected (see Kochanek 2009). The typical main sequence companion is too faint to be observed. Second, if ccSNe form dust in their ejecta (as seen, e.g., for SN 1987a, Matsuura et al. 2015), then the secondary will also be heavily dust obscured for decades (Kochanek 2017). There are several possible detections of surviving secondaries (e.g., SN 1993J, Maund et al. 2004, Fox et al. 2014, SN 2011dh, Folatelli et al. 2014 but see Maund et al. 2015, and iPTF13bvn, Bersten et al. 2014), but it is unlikely that distant ccSN can be used to carry out any census of binary companions. Moreover, it will be virtually impossible to determine if the binary is still bound.

Most observational efforts to explore the relationship between ccSNe and binaries have focused on understanding runaway B stars (e.g., Blaauw 1961, Gies & Bolton 1986, Hoogerwerf et al. 2001, Tetzlaff et al. 2011, Renzo et al. 2018) and the contribution of binary disruption to the velocities of neutron stars (e.g., Gunn & Ostriker 1970, Iben & Tutukov 1996, Cordes & Chernoff 1998, Faucher-Giguère & Kaspi 2006). Identifying stellar companions has focused on Type Ia SNe and the single versus double degenerate problem (e.g., Schweizer & Middleditch 1980, Ruiz-Lapuente et al. 2004, Ihara et al. 2007, González Hernández et al. 2012, Schaefer & Pagnotta 2012), with much less attention to finding stellar companions to ccSNe.

van den Bergh (1980) seems to have made the first

search of supernova remnants (SNRs) for runaway stars by looking for a statistical excess of O stars close to the centers of 17 Galactic SNRs and finding none. Guseinov et al. (2005) examined 48 Galactic SNRs for O or B stars using simple color, magnitude and proper motion selection cuts to produce a list of candidates, but did not investigate them in detail. Dinçel et al. (2015) identify and characterize a candidate unbound binary star in the $\sim 3 \times 10^4$ year old SNR G180.0-01.7 (S147). This SNR also contains PSR J0538+2817, and Dinçel et al. (2015) argue that the pair were likely a binary before the SN. Kochanek (2018) found that the Crab and Cas A were not binaries at the time of their explosions, finding no possible former secondaries down to mass ratios $q \lesssim 0.1$. The result for Cas A was later confirmed by Kerzendorf et al. (2018). Boubert et al. (2017) identify 4 candidates, associated with the SNRs G074.0-08.5 (Cygnus Loop), G089.0+04.7 (HB 21), G180.0-01.7 (S147, this is the same candidate as Dinçel et al. 2015), and G205.5+00.5 (Monoceros Loop).

Finding stars associated with binaries disrupted by the ccSNe is challenging because the star is no longer co-located with the compact object. Some combination of parallaxes and proper motions must be used to identify stars that are consistent with an estimate of the explosion center both spatially and temporally. Unfortunately, accurate stellar parallaxes are not a panacea because comparably accurate distances for the compact remnants and SNRs are generally lacking. The interpretation of proper motions is complicated by the difficulties in determining explosion centers, as discussed in Holland-Ashford et al. (2017).

A much simpler problem is to search for surviving binaries because the search position is exactly known from the identification of the compact remnant. Somewhat to our surprise, this exercise seems never to have been carried out and we attempt the first such survey here. This does not mean that we will have results free of ambiguities. But we will discuss these issues as we proceed, and lay out a program to address them in our conclusions. We first consider our theoretical expectations in more detail using BPS models in §2. Next we select a sample of SNRs from a combination of Ferrand & Safi-Harb (2012) and Green (2014), and search for any associated compact objects at radio, X-ray, or γ -ray wavelengths. For the SNRs where compact objects have been identified, we estimate the stellar masses for the ones which have a stellar companion and set mass limits for those which apparently do not. This process and its potential selection effects are discussed in §3. The properties of the SNRs with compact objects are discussed in Appendix A, SNRs without clearly identified compact objects are discussed in Appendix B, and rejected SNRs are discussed in Appendix C. We also examine the transverse velocities of HMXBs from the catalog of Liu et al. (2006) for comparison to the velocities of the binaries and non-binaries in the SNRs. We discuss the consequences for binaries and ccSN in §4, and outline future possibilities in §5

2 THEORETICAL EXPECTATIONS

To better frame our expectations, we use the *StarTrack* population synthesis models (Belczynski et al. 2002, 2008).

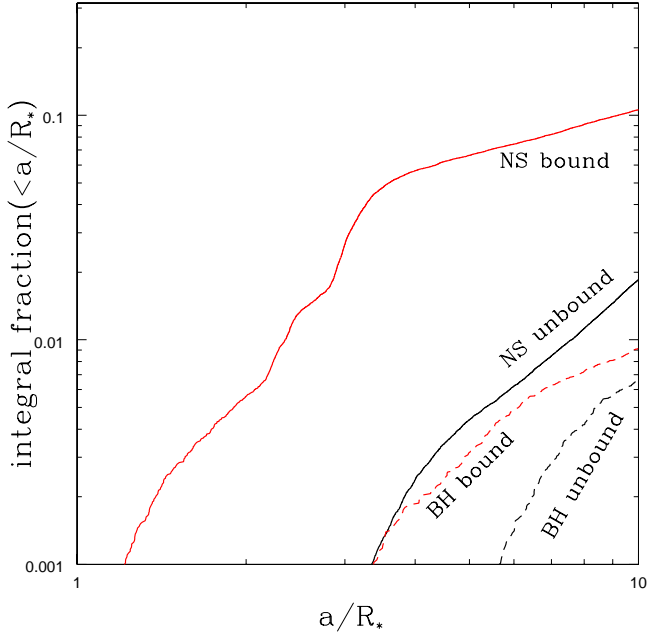


Figure 1. The integral distributions of the ratio a/R_* between the pre-SN semimajor axis a and the companion stellar radius R_* divided by whether the core collapse forms NS or a BH and whether the binary is bound or unbound afterwards.

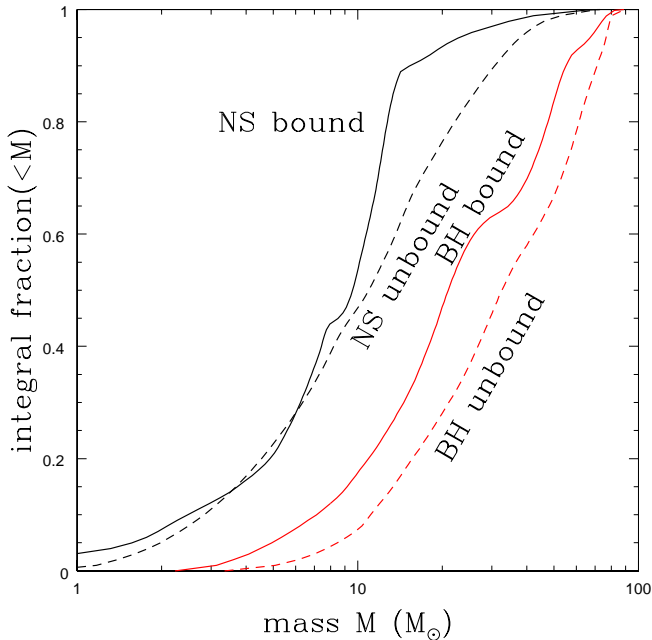


Figure 2. The integral distributions of stellar masses M for stellar companions (i.e., excluding WD, NS, BH) at the time of core-collapse, separated by the compact object formed (NS in black, BH in red) and whether the binary remains bound (solid) or unbound (dashed).

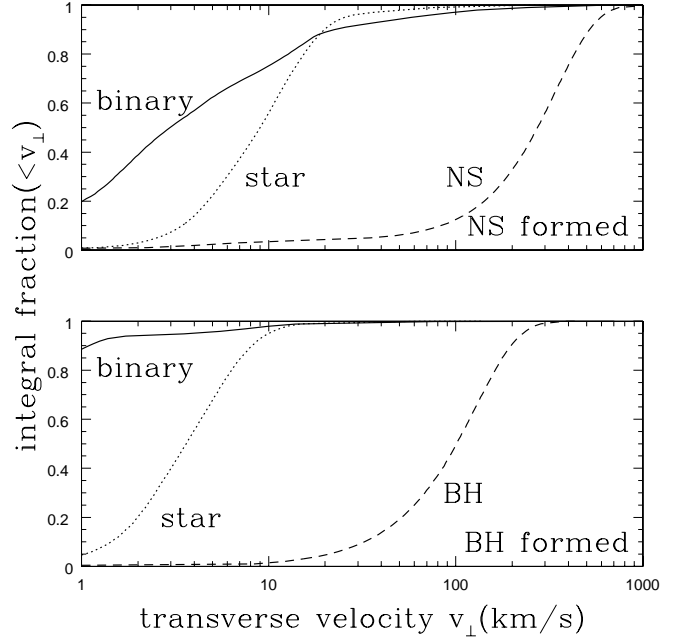


Figure 3. Integral distributions of the transverse velocities v_{\perp} after core collapse, excluding cases where the companion is a compact object, separated by whether a NS (top) or BH (bottom) is formed. These velocities are in the rest frame of the center of mass of the pre-SN binary. The three curves are for surviving binaries (solid, “binary”), unbound stellar companions (dotted, “star”), and unbound compact objects (dashed, “NS” or “BH”).

We have employed the latest version of **StarTrack**, which includes number of updates and revisions outlined below. The initial distributions of binary parameters are consistent with observations of massive O/B stars presented by Sana et al. (2012), with some minor modifications discussed in de Mink & Belczynski (2015). The IMF is a 3 component broken power law with boundaries at $M_{\text{ZAMS}} = 0.08, 0.5, 1.0,$ and $150M_{\odot}$ and slopes of $-1.3, -2.2$ and -2.3 for the three mass ranges (Kroupa & Weidner 2003). We assume a flat mass ratio distribution with $P(q)$ constant over the mass ratio range $0.1 < q = M_2/M_1 < 1$ (e.g., Kobulnicky & Fryer 2007), a binary orbital period distribution $P(\log p) \propto (\log p)^{-0.5}$ over the period range from $10^{0.15}$ to $10^{5.5}$ days, and a power-law distribution of binary eccentricities $P(e) \propto e^{-0.42}$ for $0 < e < 0.9$. We then evolve single stars and primaries with masses from $5\text{--}150M_{\odot}$, and secondaries with masses from $0.08\text{--}150M_{\odot}$ assuming a constant star formation rate and Solar metallicity ($Z = Z_{\odot} = 0.02$).

The evolutionary model adopted in our calculation corresponds to model M10 of Belczynski et al. (2017). The improvements relevant for massive star evolution include updates to the treatment of CE evolution (Dominik et al. 2012), the compact object masses produced by core collapse/supernovae (Fryer et al. 2012; Belczynski et al. 2012), and the effects of pair-instability pulsation supernovae and pair-instability supernovae (Belczynski et al. 2016).

In addition to the Blaauw (1961) effects of symmetric mass loss, including neutrinos, each NS and BH at formation is assigned a randomly oriented natal kick velocity of magnitude

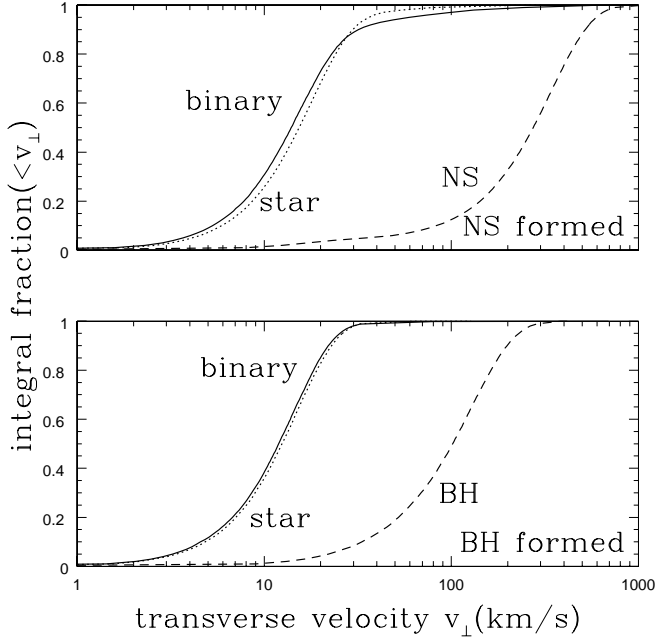


Figure 4. Integral distributions of the transverse velocities v_{\perp} measured relative to the mean motion of nearby stars assuming a 1D velocity dispersion of 10 km/s. This excludes cases where the companion is a compact object and is separated by whether a NS (top) or BH (bottom) is formed. The three curves are for surviving binaries (solid, “binary”), unbound stellar companions (dotted, “star”), and unbound compact objects (dashed, “NS” or “BH”).

$$V_{\text{NK}} = (1 - f_{\text{fb}}) \sqrt{V_x^2 + V_y^2 + V_z^2}, \quad (2)$$

where V_x , V_y , V_z are three velocity components drawn from a Maxwellian distribution with $\sigma = 265$ km/s (Hobbs et al. 2005). The fallback parameter f_{fb} describes the fraction of the stellar envelope that falls back onto the proto-compact object. Specifically, the mass of the NS or BH is calculated from

$$M_{\text{BH/NS}} = 0.9 [M_{\text{proto}} + f_{\text{fb}}(M - M_{\text{proto}})], \quad (3)$$

where $M_{\text{proto}} = 1.0M_{\odot}$ is the initial compact object mass formed in core-collapse, M is the pre-supernova mass of the star and the factor of 0.9 allows for 10% of baryonic mass loss in neutrino emission. The fallback parameter is estimated from the “rapid” supernova mechanism that is able to reproduce the observed mass-gap between NSs and BHs from Fryer et al. (2012).¹

There are two notable exceptions to this scheme for the natal kicks. First, for the most massive BHs ($M_{\text{BH}} \gtrsim 10 - 15M_{\odot}$), there is no natal kick, as there is no mass loss ($f_{\text{fb}} = 1.0$). Second, for NSs formed in electron capture supernova (ECS; Miyaji et al. 1980), we assume no natal kick, as core-collapse is predicted to be very rapid and the asymmetries needed to drive natal kicks may not develop (Dessart et al. 2006; Jones et al. 2013; Schwab et al. 2015). The effects of

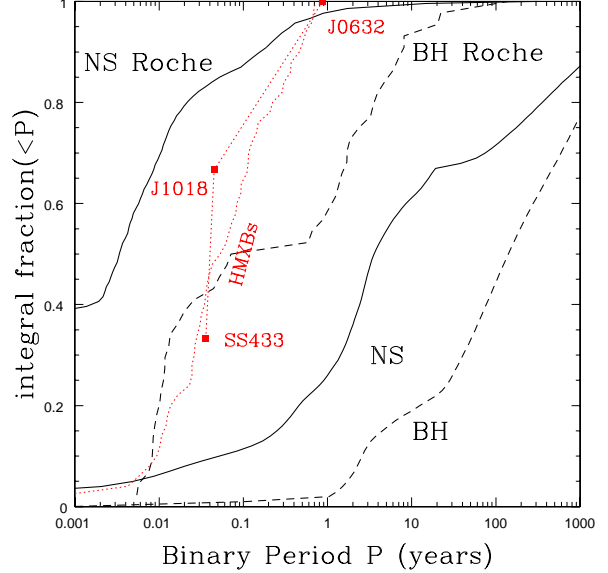


Figure 5. Integral distributions of NS (black solid) and BH (black dashed) stellar binary periods after core collapse. The curves labeled “NS/BH Roche” are the period distributions of the binaries for which the orbital pericenter lies inside the star’s Roche lobe after eliminating actual collisions. The integral period distribution of the three HMXBs associated with our sample of SNRs and of the Liu et al. (2006) catalog of field HMXBs are also shown. SS 433 is a Roche lobe accretion system, while J0632 and J1018 are wind accretion/interaction systems. The distribution of the overall HMXB population in period will be affected by the post-SN evolution of the star and binary.

neutrino mass loss are still included for both cases, as is symmetric mass loss for the electron capture SNe.

Based on these models, Table 1 summarizes the supernovae from systems that started as binaries. Roughly 34% of the ccSN associated with binaries are the explosions of merger remnants, quite similar to the $22_{-9}^{+26}\%$ found by Renzo et al. (2018). For those that are binaries at the time of explosion, we divide the sample by the remnant formed in the explosion (NS or BH) and the type of companion at the time of the explosion: main sequence (MS), evolved/stripped (EV), white dwarf (WD), NS or BH. We present the totals and then subdivide them by whether the binary is bound or unbound after the explosion. There is a very small fraction ($\sim 0.1\%$) where the remnant collides with the stellar companion after the explosion which we will not track. In the discussion that follows, we consider only the binaries in which the companion is stellar and ignore those in which the companion at the time of explosion is a compact object. We will also generally not distinguish between MS and evolved/stripped stellar companions.

Whether a stellar companion shows any peculiarities after the ccSN will strongly depend on the separation at the time of the explosion relative to the radius of the star. Figure 1 shows the distribution of the stellar binaries in the ratio a/R_* of the pre-SN semimajor axis a to the stellar radius R_* . We show the four cases corresponding to binaries which become unbound or remain bound and either NS or BH formation. We are only interested in cases where this ratio is small, and these orbits have generally circularized and

¹ The formula for the model coefficient a_1 in Eqn. 16 of Fryer et al. (2012) should read $a_1 = 0.25 - 1.275/(M - M_{\text{proto}})$.

we can ignore ellipticity. Geometrically, the star subtends fraction $R_*^2/4a^2$ of the explosion, and even for $a/R_* = 3$, only 2.8% of the ccSN energy is intercepted by the companion. In our models, only the explosions forming neutron stars with binaries that remain bound have even a small chance of being significantly impacted by the explosion, and even then it is only $\sim 1\%$ of these systems. Liu et al. (2015) estimate that 5% have $a/R_* < 5$, which is roughly consistent with Figure 1. Hence, strongly shock-impacted companions are rare.

Figure 2 shows the masses of stellar companions, again divided by the type of remnant formed and whether the binary remains bound. As expected from the simple non-interacting model and also found by Renzo et al. (2018), the typical companion is quite massive, with $\sim 88\%$ of the companions associated with the formation of an NS having $M_* > 3M_\odot$. Companions to newly formed black holes tend to be somewhat more massive.

Figure 3 shows the post-SN transverse velocities of the systems with the same divisions by outcome. For the disrupted systems, the velocities of both the star and the remnant are shown. These are velocities relative to the pre-SN binary center of mass and would be applicable for motions relative to the center of the SNR or the relative motions of unbound systems. Like Renzo et al. (2018), we find that the stars move surprisingly slowly. For the NS case, 90% of the bound (unbound) stars moving more slowly than 23 km/s (20 km/s). For the BH case the velocities are still lower, with 90% of the bound (unbound) stars moving more slowly than 1 km/s (8 km/s). While the typical binary moves more slowly than the typical unbound star, there is a high velocity tail to the binary distribution.

In §3 we measure transverse velocities relative to the rest frame defined by nearby stars. These transverse velocities will include the pre-SN motion of the binary relative to nearby stars. The typical one-dimensional velocity dispersion of O stars is 10 km/s (see, e.g., Binney & Merrifield 1998), so we add Gaussian deviates with this amplitude to the velocity vectors from the BPS models. This leads to the velocity distribution shown in Figure 4. It is now quite difficult to discern any differences in the stellar velocities by binary status, although the systems associated with forming a BH still have markedly lower velocities. For the bound and unbound NS (BH) systems, 90% of the velocities are less than 32 km/s (22 km/s) and 30 km/s (23 km/s), respectively. We should note that Renzo et al. (2018) discuss the statistics of runaway stars unassociated with SNRs using the pre-SN binary frame (Figure 3) when they should be using velocities in the local stellar rest frame (Figure 4).

Finally, Figure 5 shows the period distribution of the surviving star plus NS or BH binaries. Using the standard approximations for the size of the Roche lobe (e.g., Paczyński 1971), we also show the period distribution of the binaries that have pericenters with Roche lobes smaller than the stellar radius. These are the systems which can be mass transfer binaries immediately after the explosion. They are relatively rare, consisting of 3.6% of the NS binaries and 0.1% of the BH binaries. These could be underestimated if the impact of the explosion or a sudden increase in the tidal forces on the star drive it to expand on a short time scale.

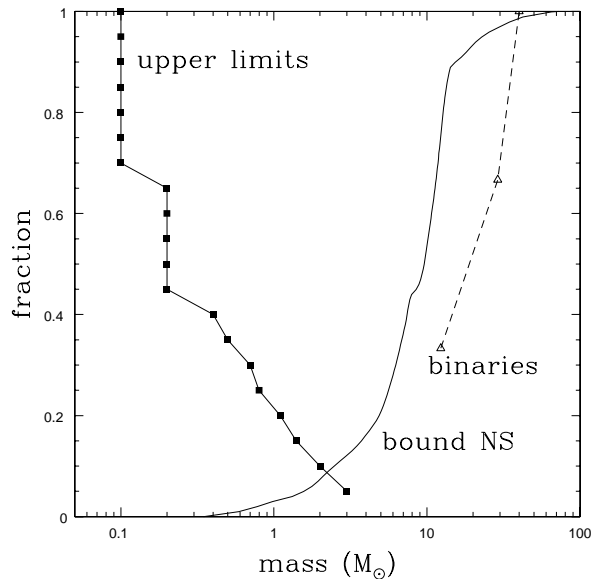


Figure 6. The integral distributions of the three binary masses (dashed, triangles) and the 20 upper limits (solid, squares) for the SNRs with clearly associated compact remnants. For comparison, the mass distribution of bound NS binaries in our BPS models from §2 is also shown.

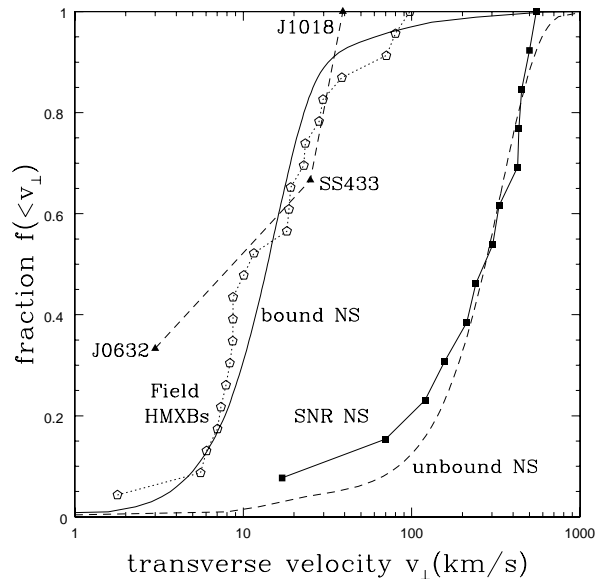


Figure 7. The integral distributions of the three binary transverse velocities (dashed, triangles) and the non-binary NS transverse velocities (solid, squares). For comparison, we also show the transverse velocities of field HMXBs from the catalog Liu et al. (2006). Since HMXBs are short lived, their velocities are little affected by their post-SN Galactic orbit and should be directly comparable to the binaries in the SNRs. The transverse velocity distributions of bound star/NS binaries and unbound NS from our BPS models in §2 are also shown. These include an additional velocity dispersion of $\sigma = 10$ km/s for each velocity component because we are measuring the transverse velocities relative to the local stars (i.e., Figure 4 rather than Figure 3).

Table 1. ccSN From Initial Binaries By Outcome

Outcome	Total	Single	Binary
Merger	0.338	–	–
NS+MS	0.230	0.200	0.029
NS+EV	0.014	0.010	0.003
NS+WD	0.041	0.028	0.013
NS+NS	0.177	0.171	0.006
NS+BH	0.026	0.025	0.001
BH+MS	0.044	0.021	0.024
BH+EV	0.005	0.002	0.002
BH+WD	0.000	0.000	0.000
BH+NS	0.075	0.075	0.000
BH+BH	0.049	0.039	0.010

For the explosions in binaries, the first entry is the compact object being formed and the second entry is the binary companion at the time.

3 SAMPLE

To build our sample of SNRs, we started with the Manitoba data base of SNRs (Ferrand & Safi-Harb 2012). In practice, this data base is a mixture of SNRs and pulsar wind nebulae (PWN), so we also required the SNR to be in the SNR catalog of Green (2014). Next we required the SNR to have a reported distance that could be closer than 5 kpc. Where possible, we required an X-ray estimate of the column density $N(H) < 10^{22} \text{ cm}^{-2}$. If no X-ray estimate was available, we required a total Galactic $A_V < 5$ mag based on Schlafly & Finkbeiner (2011). We assume a relation between $N(H)$ and extinction of $E(B-V) = 1.7N(H) \times 10^{-22}$ (Bohlin et al. 1978). For $R_V = 3.1$, $N(H) = 10^{22} \text{ cm}^{-2}$ corresponds to $A_V = 5.3$ mag or $E(B-V) = 1.7$. These criteria led to an initial list of 54 SNRs.

We then investigated the individual SNRs in detail and divided them into three categories. First, there are 23 SNRs with clearly associated compact objects identified as either radio pulsars, X-ray sources or γ -ray sources. Second, there are 26 SNRs without clearly associated compact objects. This includes cases with X-ray fluxes below $10^{-13} \text{ erg cm}^{-2} \text{ s}^{-1}$ where there are generally multiple candidates for an associated compact object, but too few counts to determine their nature. Finally, there are 5 SNRs which are dropped. In four cases, they are SNRs associated with Type Ia SNe (Kepler, Tycho, G315.4–02.3 and G327.6+14.6), and in one case (G011.1+00.1) the distance in the data base is for a NS in the foreground of a significantly more distant SNR. Appendix A summarizes the properties of the SNRs with clearly associated compact objects, Appendix B summarizes those without, and Appendix C summarizes the rejected SNRs. Of the sample with compact objects, 8, 12 and 3 were *first* identified as radio, X-ray and γ -ray sources, respectively. Three of these sources, SS 433 (see the review by Margon 1984), HESS J0632+057 (Hinton et al. 2009) and 1FGL J1018.6–5856 (Corbet et al. 2011), are known binaries.

For each of the accepted SNRs we searched for prior optical or near-IR studies of the compact object. If none were available, we searched for the source in other catalogs, in particular, PanSTARRS (Chambers et al. 2016), 2MASS (Skrutskie et al. 2006), UKIDSS (Lucas et al.

2008), APASS (Henden et al. 2016) and Gaia DR2 (Gaia Collaboration et al. 2018). We adopted distance estimates from the literature, supplemented by the Gaia parallaxes of the known binaries. For many of the sources we could check the X-ray estimate of the extinction based on the hydrogen column density $N(H)$ against the PanSTARRS 3D dust distribution models of Green et al. (2015). The two extinction estimates generally agreed reasonably well. These distance and extinction estimates were converted into the rough priors given in Table 2. We assume minimum extinction uncertainties of 0.1 mag. To interpret the magnitudes, we used Solar metallicity PARSEC v1.2S (Chen et al. 2015) isochrones sampled in $\log(\text{age}/\text{years})$ from 6.0 to 7.5 increments of 0.01 dex. Note that at these young ages, the lower mass stars are not on the main sequence when the primary explodes – they are significantly more luminous pre-main sequence stars.

For the sources without stellar companions, we use the optical and near-IR fluxes or flux limits to set upper bounds on the mass of any stellar companion. Some of the systems (e.g., the Crab, see Appendix A) have optical/near-IR counterparts due to emission from the NS and we simply use these fluxes as upper limits. Given an apparent magnitude m_i and a model absolute magnitude M_i for filter i , we have that $m_i = M_i + \mu + R_i E(B-V)$ where we use the PARSEC estimates of R_i for each filter based on a Cardelli et al. (1989) $R_V = 3.1$ extinction curve. Given the distance (modulus) prior ($\mu_0 \pm \sigma_\mu$), the extinction prior ($E_0 \pm \sigma_E$) and the relation between apparent and absolute magnitudes, we optimize the goodness of fit statistic

$$\chi^2 = \left(\frac{\mu - \mu_0}{\sigma_\mu} \right)^2 + \left(\frac{E - E_0}{\sigma_E} \right)^2$$

to estimate the distance modulus μ and extinction E for each model star on the isochrones. Because the fits are under-constrained, essentially having two constraints (on μ and E) for four variables (μ , E , temperature T_* and luminosity L_*), there are always solutions with $\chi^2 = 0$. As a conservative bound on the mass, we find the maximum mass for each filter which satisfies $\chi^2 < 4$, and then report in Table 2 the magnitude limit for the most constraining filter and the associated maximum mass. Generally, other similar filters (e.g., J and H if the best limit came from K) give similar but slightly weaker constraints.

The constraints on distance and extinction in Table 2 are designed to roughly cover the range of values and uncertainties found in our survey of the literature for each source. Despite the somewhat uncertain nature of the estimates for many sources, our results are robust to reasonable changes in these estimates for two reasons. First, we are not particularly interested in the difference between a mass limit of (for example) $0.2M_\odot$ and $0.4M_\odot$. As outlined in the introduction and discussed further in §2, all that really matters is that the source cannot have a (say) $3M_\odot$ stellar counterpart since this already encompasses a large fraction of the expected secondary population. Second, particularly for this level of accuracy, the mass estimates are robust to changes in distance or extinction because luminosity is a steep function of mass for (pre-)main sequence stars, $L \propto M^x$ with $x \simeq 2-3$. Since L depends on distance as d^2 , the mass depends on distance as $M \propto d^{2/x}$ and even a factor of two change in distance changes the mass by only 60% for $x = 3$.

Table 2. Limits on Companions

SNR	Compact Source	Discovery	d (kpc)	$E(B - V)$ (mag)	Limit (mag)	Mass (M_{\odot})	v_{\perp} (km/s)	Known Binary
G034.7–00.4	J1856+0113	radio	3.0 ± 0.5	2.2 ± 0.7	$H > 19.0$	< 0.7	...	
G039.7–02.0	SS 433	radio	5.0 ± 0.7	1.9 ± 0.9	...	12.3 ± 3.3	25 ± 8	Yes
G065.7+01.2	J1952.2+2925	X-ray	3.0 ± 2.0	0.7 ± 0.5	$z > 18.2$	< 3.0	...	
G069.0+02.7	PSR B1951+32	radio	2.0 ± 0.5	0.5 ± 0.2	$V > 24.3$	< 0.5	240 ± 40	
G078.2+02.1	PSR J2021+4026	γ -ray	1.5 ± 0.5	1.3 ± 0.3	$H > 19.0$	< 0.2	~ 550	
G106.3+02.7	PSR J2229+6114	radio	3.0 ± 1.0	1.1 ± 0.2	$R > 23$	< 0.8	...	
G109.1–01.0	AXP 1E 2259+586	X-ray	4.1 ± 0.7	1.3 ± 0.4	$K > 21.7$	< 0.1	157 ± 17	
G111.7–02.1	Cas A	X-ray	3.4 ± 0.3	1.7 ± 0.9	$J > 26.2$	< 0.1	~ 330	
G114.3+00.3	PSR B2334+61	radio	3.2 ± 1.7	1.0 ± 0.7	$z > 22.3$	< 1.1	212 ± 268	
G119.5+10.2	PSR J0007+7303	X-ray	1.4 ± 0.3	0.5 ± 0.1	$r > 27.6$	< 0.1	~ 450	
G130.7+03.1	PSR J0205+6449	X-ray	4.5 ± 1.6	0.7 ± 0.1	$i > 25.5$	< 0.2	17 ± 9	
G180.0–01.7	PSR J0538+2817	radio	1.5 ± 0.4	0.5 ± 0.1	$z > 22.3$	< 0.2	425 ± 94	
G184.6–05.8	Crab	radio	2.5 ± 0.5	0.5 ± 0.1	$J > 14.8$	< 2.0	~ 120	
G189.1+03.0	CXO J061705.3+222127	X-ray	1.7 ± 0.3	1.2 ± 0.1	$z > 22.3$	< 0.2	~ 500	
G205.5+00.5	HESS J0632+057	γ -ray	1.8 ± 0.2	0.6 ± 0.1	fit	20-36	3 ± 1	Yes
G260.4–03.4	PSR J0821–4300	X-ray	1.3 ± 0.3	0.5 ± 0.1	$I > 25.6$	< 0.1	433 ± 126	
G263.9–03.3	Vela	radio	0.29 ± 0.02	0.1 ± 0.1	$R > 23.9$	< 0.1	70 ± 8	
G266.2–01.2	CXOU J085201.4–461753	X-ray	0.7 ± 0.2	0.5 ± 0.2	$R > 25.6$	< 0.1	...	
G284.3–01.8	1FGL J1018.6-5856	γ -ray	5.4 ± 3.0	1.5 ± 0.2	fit	29-61	39 ± 7	Yes
G291.0–00.1	CXOU J111148.6–603926	X-ray	5.0 ± 2.0	1.1 ± 0.1	$G > 22$	< 1.4	303 ± 130	
G296.5+10.0	PSR J1210–5226	X-ray	2.1 ± 1.8	0.2 ± 0.1	$R > 27.1$	< 0.2	...	
G320.4–01.2	PSR J1513–5908	X-ray	5.2 ± 1.4	1.5 ± 0.2	$H > 20.6$	< 0.4	...	
G332.4–00.4	1E 161348–5055	X-ray	3.1 ± 0.5	1.7 ± 0.7	$K_s > 22.1$	< 0.1	...	

The Type column indicates the discovery method. The distance, d , and extinction, $E(B - V)$, columns are rough summaries based on the discussion of each object in Appendix A. As discussed in §3, the results are robust to reasonable changes in these estimates. The Mag column gives the most constraining magnitude limit on the presence of a stellar companion, excluding the three known binaries. The Mass column is the upper mass limit implied by the magnitude limit or a mass estimate for the stellar companion in the binary. For SS 433 we use the mass from Hillwig & Gies (2008). The transverse velocity measurements or limits are given in the v_{\perp} column, and the Known Binary column flags the known binaries.

Similarly, L depends on extinction as $10^{R_i E/2.5}$, so the mass depends on extinction as $10^{R_i E/2.5x}$. For $x = 3$, changing the extinction $E(B - V)$ by 1 magnitude, changes the mass by a factor of ~ 2.2 at R band (effectively the bluest filter used in Table 2), but only by 30% at J band and 11% at K.

A different procedure is required for the actual binaries. For HESS J0632+057 and 1FGL J1018.6-5856 we fit the spectral energy distributions (SED) using the PARSEC models, adding a spectroscopic temperature prior and a Gaia parallax prior (see Appendix A). We did this by fitting the photometry with the priors on distance and extinction given in Table 2 and then adding terms to the χ^2 for parallax ($\pi \pm \sigma_{\pi}$) and temperature ($T \pm \sigma_T$). This treatment of the distance and the parallax is imperfect, but there is no need to do a more complex non-linear fit for our purposes. For HESS J0632+057 we get a mass of $29M_{\odot}$ ($20M_{\odot} < M < 36M_{\odot}$), somewhat larger than the estimate of $13M_{\odot} < M < 19M_{\odot}$ by Aragona et al. (2010). The difference is likely that Aragona et al. (2010) correct for a significant amount of disk emission, while we did not. For 1FGL J1018.6-5856, we get $40M_{\odot}$ ($29M_{\odot} < M < 61M_{\odot}$) while Napoli et al. (2011) find $31M_{\odot}$. The optical and near-IR emission of SS 433 is completely dominated by accretion, and there is some debate over the mass of the star. For our study, we simply adopt the estimate by Hillwig & Gies (2008) of $(12.3 \pm 3.3)M_{\odot}$. The mass limits and binary masses are shown in Figure 6.

Where possible, we also include estimates of the trans-

verse velocity v_{\perp} in Table 2. Many come from the offset of the source from the geometric or expansion center of the SNR, while others are from actual proper motion measurements (see Appendix A). Holland-Ashford et al. (2017) has a good discussion of the reliability of these estimates. For our purposes, we are interested in the order of magnitude of the velocities rather than their precise values. Where there are proper motion measurements, we used Gaia DR2 proper motions of stars near the estimated distance of the compact object to empirically determine the local standard of rest without any reference to a kinematic model for the Galaxy.

In particular, for the three binaries, we compare the Gaia DR2 proper motion of each binary to stars whose parallax is within 1σ of the binary's parallax. We used a search region (5 to 30 arcmin) centered on the source that was large enough to include 1000 to 2000 stars meeting the parallax criterion. We then computed the proper motion of the stars and the dispersion of the proper motions around the mean. The transverse velocity is then the motion of the binary minus the local mean multiplied by the distance determined from the parallax, with an uncertainty determined by the standard propagation of errors. If we use the same procedure for the pulsars with VLBI parallaxes, we find results consistent with previously measured transverse velocities using Galactic kinematic models to define the local standard of rest. Table 2 and Figure 7 use our estimates of v_{\perp} .

Since all three binaries in our sample are HMXBs, we carried out a similar analysis of the transverse velocities of

Table 3. HMXB Transverse Velocities

HMXB	Gaia ID	v_{\perp} (km/s)	π (mas)	$PMRA$ (mas/year)	$PMDec$ (mas/year)	N_*	$\langle PMRA \rangle$ (mas/year)	$\langle PMDec \rangle$ (mas/year)
1H 1253–761	5837600152935767680	19 ± 1	4.70 ± 0.03	−27.18 ± 0.06	−9.02 ± 0.05	1499	−10.42 ± 13.62	−0.40 ± 7.43
1H 1249–637	6055103928246312960	10 ± 1	2.38 ± 0.12	−12.51 ± 0.16	−3.98 ± 0.15	1737	−8.72 ± 7.94	−0.67 ± 4.66
2S 1145–619	5334823859608495104	6 ± 1	0.42 ± 0.04	−6.22 ± 0.05	1.46 ± 0.05	1948	−6.71 ± 2.61	1.24 ± 1.73
4U 1258–61	5863533199843070208	28 ± 3	0.47 ± 0.03	−4.23 ± 0.04	−0.32 ± 0.05	260	−6.98 ± 3.21	−0.77 ± 1.90
1H 1255–567	6060547331128876928	11 ± 1	8.95 ± 0.23	−28.15 ± 0.22	−10.34 ± 0.34	1525	−9.11 ± 18.94	0.11 ± 12.31
1H 1555–552	5884544931471259136	7 ± 0	0.72 ± 0.04	−3.11 ± 0.06	−3.29 ± 0.05	1359	−3.86 ± 3.49	−4.04 ± 2.83
1H 0739–529	5489434710755238400	8 ± 1	1.53 ± 0.04	−4.53 ± 0.09	8.60 ± 0.09	1324	−3.22 ± 6.42	6.15 ± 8.66
1WGA J0648.0–4419	5562023884304074240	8 ± 1	1.97 ± 0.06	−4.11 ± 0.11	5.67 ± 0.12	1875	−0.60 ± 8.00	4.94 ± 13.37
4U 0900–40	620657678322625920	70 ± 7	0.38 ± 0.03	−4.96 ± 0.05	9.09 ± 0.05	1470	−4.09 ± 2.37	3.46 ± 2.54
4U 1700–37	5976382915813535232	80 ± 9	0.55 ± 0.06	2.22 ± 0.09	4.95 ± 0.07	1705	−2.02 ± 3.12	−3.25 ± 3.00
RX J1744.7–2713	4060784345959549184	8 ± 1	0.83 ± 0.06	−0.96 ± 0.10	−2.06 ± 0.08	1301	−1.88 ± 3.92	−3.26 ± 3.81
IGR J17544–2619	4063908810076415872	22 ± 3	0.35 ± 0.05	−0.65 ± 0.08	−0.53 ± 0.07	1827	−0.53 ± 2.30	−2.22 ± 2.58
RX J1826.2–1450	4104196427943626624	97 ± 10	0.48 ± 0.05	7.43 ± 0.09	−8.00 ± 0.07	1514	−0.99 ± 2.33	−2.77 ± 2.81
XTE J1901+014	4268294763117802368	38 ± 4	0.64 ± 0.08	−4.07 ± 0.11	−7.53 ± 0.10	1737	−0.88 ± 3.16	−3.49 ± 3.97
1A 0535+262	3441207615229815040	18 ± 2	0.44 ± 0.05	−0.63 ± 0.09	−3.04 ± 0.07	1361	0.92 ± 1.90	−2.27 ± 2.42
1H 0556+286	3431561565357225088	8 ± 1	0.39 ± 0.06	0.61 ± 0.11	−2.72 ± 0.09	1553	0.72 ± 1.78	−2.05 ± 2.15
4U 0352+309	168450545792009600	18 ± 1	1.23 ± 0.06	−1.40 ± 0.10	−2.25 ± 0.07	1963	2.67 ± 6.08	−4.63 ± 5.79
4U 1956+35	2059383668236814720	23 ± 2	0.42 ± 0.03	−3.88 ± 0.05	−6.17 ± 0.05	1305	−2.41 ± 2.16	−4.72 ± 2.84
EXO 051910+3737.7	84497471323752064	7 ± 1	0.75 ± 0.06	1.44 ± 0.12	−4.12 ± 0.07	1870	1.32 ± 2.79	−2.87 ± 3.31
RX J2030.5+4751	2083644392294059520	7 ± 1	0.37 ± 0.03	−3.05 ± 0.05	−4.62 ± 0.05	1388	−2.61 ± 2.34	−4.24 ± 2.76
1H 2202+501	1979911002134040960	29 ± 3	0.84 ± 0.04	2.40 ± 0.07	−0.27 ± 0.07	1112	−2.09 ± 4.25	−2.97 ± 3.68
1E 0236.6+6100	465645515129855872	1 ± 0	0.38 ± 0.04	−0.30 ± 0.04	−0.08 ± 0.07	1903	−0.22 ± 1.89	−0.20 ± 1.87
RX J0146.9+6121	511220031584305536	5 ± 0	0.37 ± 0.03	−0.88 ± 0.03	0.03 ± 0.04	1599	−0.92 ± 1.70	−0.40 ± 1.47

For each HMXB we give the associated Gaia ID, the final estimate of the transverse velocity v_{\perp} , the Gaia parallax (π), the proper motions in RA ($PMRA$) and Dec ($PMDec$), the number of stars N_* used to define the local standard of rest, and the mean and dispersion of the proper motions of these stars in RA ($\langle PMRA \rangle$) and Dec ($\langle PMDec \rangle$). The uncertainty in the mean proper motion is smaller than the dispersion by $(N_* - 1)^{-1/2}$.

Table 4. Estimated Binary Fractions f

Case	N_b	N_s	median	90% conf	comments
Non-Interacting NS	0	23		< 0.091	< $3M_{\odot}$
	0	22		< 0.095	< $2M_{\odot}$
	0	21		< 0.099	< M_{\odot}
Interacting BH	1	22	0.069	0.012-0.18	no bias
	1	42	0.038	0.008-0.10	naive Ia
	1	48	0.033	0.006-0.09	full bias
Interacting NS	2	21	0.109	0.035-0.24	no bias
	2	41	0.060	0.019-0.14	naive Ia
	2	47	0.053	0.017-0.12	full bias
Interacting BH/NS	3	20	0.151	0.059-0.29	no bias
	3	40	0.083	0.032-0.17	naive Ia
	3	46	0.082	0.032-0.17	full bias

HMXBs from the catalog of Liu et al. (2006). The catalog contains 114 binaries, 67 of which have an optical magnitude. Of these, we found good matches in Gaia DR2 for 57 and we kept the 23 with $V < 19$ mag, parallaxes larger than 0.333 mas (i.e., $d < 3$ kpc), and parallax errors at least 5 times smaller than the parallax. As with the binaries in the SNRs, we then selected $N_* = 1000$ -2000 nearby stars with parallaxes within 1σ of the parallax of the binary to define the local standard of rest and defined the transverse velocity of the binary by the difference between the proper motion of the binary and the mean proper motion of the nearby stars. These estimates are given in Table 3.

4 RESULTS

Figure 6 shows the resulting distribution of binary masses and upper limits for our sample of 23 SNRs with remnants. All three binaries are HMXBs and we find no low mass companions. SS 433 is a Roche lobe accretion system, and the other two are X-ray and γ -ray sources due to interactions between the stellar and pulsar winds. If we have N_b binaries and N_s non-binaries, then the probability distribution for the binary fraction f is the binomial distribution

$$\frac{dP}{df} \propto f^{N_b} (1-f)^{N_s}. \quad (4)$$

We can make several choices for N_b . First, the systems we can find are non-interacting NS binaries and interacting NS or BH binaries. We cannot find non-interacting BH binaries with our search procedures. Second, the γ -ray binaries are believed to be NS systems, while SS 433 is likely a BH binary (see, e.g., Hillwig & Gies 2008 for a discussion). The case $N_b = 0$ provides an upper limit on the fraction of SNRs with non-interacting NS binaries, the case $N_b = 1$ constrains the fraction with interacting BH binaries, the case $N_b = 2$ constrains the fraction of SNR with interacting NS binaries, and, finally, the case $N_b = 3$ constrains the fraction of SNRs with interacting binaries

We also have to decide on the value of N_s . This matters in three contexts. First, our upper mass limits are not uniform, so if we consider lower mass limits we have fewer SNRs where data with the necessary depth exists. Second, we looked at 49 remnants but were only able to clearly identify compact objects to check for stellar companions in 23. The

latter point should only be an issue for the interacting binaries since the failure to identify a compact remnant should have no consequences for our selection of non-interacting binaries. Third, some of these 49 remnants are probably due to Type Ia SNe. Based on local volumetric rates (e.g., comparing Horiuchi & Beacom 2010 and Horiuchi et al. 2011), the Type Ia rate is roughly 20% of the ccSN rate, although there remain significant uncertainties. We are also looking at SNRs, not SNe, and SNRs from different types of SNe will have different lifetimes (e.g., Sarbadhicary et al. 2017). We will consider the consequences of a “naive” Type Ia correction by assuming that 20% of the remnants are due to Type Ia SNe. However, we should take 20% of 53 SNR because we already rejected 4 SNR for being Type Ia. So roughly, we expect 10 Type Ia remnants, 4 of which are already recognized, leaving 6 hiding amongst the 49.

For the non-interacting binaries, we need to select a companion mass limit. The simplest possibility is simply to set a limit on the fraction with $M_* > 3M_\odot$, corresponding to the weakest mass limit in Table 2. In our BPS models, 12% of surviving companions are less massive than $3M_\odot$ (see Fig. 2). If we want to make an estimate for lower masses, we must drop remnants with weaker limits. So for $M_* > 2M_\odot$ ($> 1M_\odot$) we must drop 1 (2) systems to have $N_s = 22$ (21). Here we assume that the Crab and PSR B2334+61 are not binaries independent of the mass limits in Table 2 because they are radio pulsars without timing residuals interpreted as due to binarity (see Appendix A). In practice, the mass limit for the Crab in Table 2 could also be made much stricter by subtracting a model for the non-thermal emissions of the pulsar. In the BPS models only 7% (3%) of bound companions are below these mass limits.

Interacting binaries have enhanced high energy emission and are more detectable, so the sample of 23 SNRs with compact objects likely contains all the interacting binaries in the full sample of 49 SNRs. This suggests that we should then use $N_s = 49 - N_b$ for the statistics of the interacting binary cases. However, we also consider a “naive” Type Ia correction where we assume that 6 of the remaining SNRs are unidentified Type Ia remnants so that $N_s = 43 - N_b$.

Table 4 summarizes all these cases and gives the resulting estimates of the binary fraction f from Eqn. 4. For the cases with the interacting binaries we present the results assuming an underlying samples size of 23 (“no bias”), the full sample but contaminated by 6 Type Ia remnants (“naive Ia”), and the full initial sample (“full bias”). For $N_b = 0$ we derive a 90% confidence upper limit, and for $N_b > 0$ we derive symmetric 90% confidence limits. This does make the upper limits for the two cases look qualitatively different, because the first case has 10% of the likelihood at higher values of f and the second case has only 5%.

For the non-interacting cases we give the results for three mass limits, $M_* > 3, 2$ and $1M_\odot$. If you use the BPS models to correct for the missing lower mass systems, the limits from Table 4 become $f < 0.097, 0.098,$ and 0.102 , so we will adopt $f \lesssim 0.10$ as our fiducial, completeness-corrected estimate. For the interacting cases, we will use the “naive Ia” results as the fiducial values, because there must be some Type Ia SNR contamination and as a compromise between “no bias” and “full bias”. The estimates of $f = 0.15, 0.083$ and 0.082 for the median fraction of core collapse SNRs with interacting binaries in the “no bias”,

“naive Ia” and “full bias” are all mutually consistent given the overall uncertainties.

Figure 7 shows the distribution of the binaries and single NSs in transverse velocity simply using the nominal values from Table 2. The single NSs show the broad distribution of velocities that drives the need for a kick velocity produced by the ccSN explosion. The 3 HMXBs, on the other hand, have very small transverse velocities, and this is also true of the HMXBs from the Liu et al. (2006) catalog. This was noted previously for a smaller number of systems with Hipparcos measurements (Chevalier & Ilovaisky 1998) and by the distances between HMXBs and star clusters in the Magellanic Clouds (Coe 2005). Because these high mass stars are short lived compared to Galactic orbital periods, the transverse velocity distributions of the field HMXBs are likely quite similar to their natal values.

In Figure 7 we also show the transverse velocity distribution of the unbound NS and the star/NS binaries from the BPS models. We are measuring the transverse velocities relative to a rest frame defined by the local stars, while the BPS model velocities in Figure 3 are measured relative to the pre-SN rest frame of the binary. To model the observations, we add a velocity dispersion of 10 km/s to each velocity component from the BPS models to include the typical random velocities of young stars relative to the local mean motion (see, e.g., Binney & Merrifield 1998). The parameters of the BPS models were tuned to agree with studies of NS kicks, so it is not surprising that the match to the velocities of the unbound NS in SNRs is quite good. The agreement with the velocities of both the binaries in the SNRs and the more general HMXB population is also good even though the parameters were not optimized to produce the agreement. If the extra velocity dispersion is not included, the model distribution has too many low velocity stars compared to the observed distribution (compare Figures 3 and 7).

5 DISCUSSION

In a sample of 23 SNRs with compact remnants and 26 where none have been confidently identified, we find three surviving stellar binaries. All three are interacting, with two NS wind interaction systems, and one BH Roche accretion system. This implies (1) that the median fraction of SNRs from ccSNe with non-interacting stellar companions is $f < 0.10$; (2) that the median fraction with interacting BH companions is $f = 0.038$ ($0.008 < f < 0.10$); (3) that the median fraction with interacting NS companions is $f = 0.060$ ($0.019 < f < 0.14$); and (4) and the median fraction with either is $f = 0.83$ ($0.032 < f < 0.17$). These are all 90% confidence intervals. These are our fiducial estimates, but the variant cases discussed in §4 and Table 4 are all broadly consistent.

The observational estimates can be compared to the BPS estimates in Table 1. In the BPS models, the fraction of initial binary systems that leave a star plus compact object binary after a ccSNe is 6%, with nearly equal numbers of NS and BH systems. We cannot directly compare this with Renzo et al. (2018) because they do not subdivide the surviving bound systems by type. If we consider all bound systems, they find that 11% of SN leave some kind of binary, while we find 15%. Finally, we have to dilute the expected

number of SNRs containing stellar binaries for the binary fraction. If the initial binary fraction is $F_0 = 0.84$ based on Moe & Di Stefano (2017), then 5% of SNRs from ccSNe should contain a surviving stellar binary. This is consistent with the observations.

It does seem surprising that all three binaries in the sample are interacting. Our crude estimate in §2 is that very few surviving binaries should be close enough to immediately begin (Roche) mass transfer after the SN, which makes SS 433 somewhat of a statistical anomaly. The collision of the debris with the companion star can lead to a rapid expansion of the outer layers of the star (e.g., Liu et al. 2015), which would increase the probability of interactions while also implying that the star is out of equilibrium. The two interacting NS binaries are less problematic. Wind interaction systems can be more widely separated, and it seems plausible that interactions with the SN debris can lead the secondary to have stronger winds than normal.

The counterpart to searching for surviving binaries is to search for disrupted binaries. These should be much more common than surviving binaries. In our BPS models, 23% of the initial binary population become unbound star plus compact object binaries after the explosion. If the binary fraction is 84%, this implies that 19% of SNRs from ccSNe should contain a surviving, unbound stellar companion. Renzo et al. (2018) find a higher central fraction (58%). The range for this fraction cannot be directly estimated from Renzo et al. (2018), but it is likely large enough to encompass our value. Kochanek (2018) considered 3 core collapse SNRs (Cas A, the Crab and SN 1987A), finding that there could be no unbound stellar companions with mass ratios $q \gtrsim 1$. This implies a 90% confidence limit on the fraction with unbound stellar companions of $f < 0.44$ that is consistent with the BPS models. Four candidates for unbound stellar companions have been identified in the SNRs G074.0–08.5 (Cygnus Loop, Boubert et al. 2017), G089.0+04.7 (HB 21, Boubert et al. 2017), G180.0–01.7 (S147, Dinçel et al. 2015, Boubert et al. 2017), and G205.5+00.5 (Monoceros Loop, Boubert et al. 2017). Since the NS in G205.5+00.5 is in an HMXB (Hinton et al. 2009), it seems unlikely that the identification of a disrupted binary companion in this SNR can be correct. Cas A, the Crab, G180.0–01.7 and G205.5+00.5 are included in the present study, and if we view this as the detection of one unbound companion in a sample of 4 SNRs, then the fraction of SNRs containing unbound binaries is $f = 0.31$ ($0.076 < f < 0.66$). In total, Boubert et al. (2017) looked at 10 SNRs, and if all 3 candidate companions other than the one in G205.5+00.5 are real, and we assume the search was “complete”, then $f = 0.32$ ($0.14 < f < 0.56$). In short, while the results are all very tentative, the implications of these studies are all broadly consistent with the expectations from BPS models (e.g., §2, Renzo et al. 2018).

The three binaries present in the sample have absolute magnitudes of $M_V \sim -7$ (SS 433), -5 (HESS J0632+057) and -6 (1FGL J1018.67–5856), respectively. These are bright enough to be identifiable in nearby galaxies (18–20 mag at 1 Mpc and 23–25 mag at 10 Mpc) modulo the problem of dust formed in the ejecta heavily obscuring them in young ($< 10^2$ year) SNRs (Kochanek 2017). Their X-ray fluxes would be too faint for current X-ray observatories to detect them at these distances.

Finally, we should discuss the limitations to the present study and how they might be reduced. The optical and near-IR photometry to search for the stellar counterparts is not a major limitation. All of the weak upper limits in Table 2 are cases where we have relied on survey data rather than deep targeted observations. There would be little difficulty in obtaining new observations to drive all the upper mass limits to be significantly less than a Solar mass. Uncertainties due to extinction are already modest, and replacing all the optical limits with near-IR limits would eliminate extinction uncertainties as a consideration.

The properties of the SNRs are more problematic. The uncertainties in distance are generally more important than any uncertainties in extinction, particularly if all optical limits are replaced by near-IR limits. Since most of the SNRs contain X-ray or γ -ray sources rather than radio pulsars, there is only modest room to improve matters with VLBI parallaxes. Aside from the actual binaries, the compact objects are too faint (if detected at all) for Gaia parallaxes. Optical spectroscopy of blue stars with Gaia parallaxes could be used to better constrain the distances to the SNRs because the SNR produces absorption lines in the spectra of background stars. This has been used to search for single degenerate companions in the Type Ia Tycho remnant (e.g., Ihara et al. 2007). Blue stars are required because the absorption features all lie shortward of 4000\AA , which means this approach will be limited by foreground extinction.

It would also be helpful to have determined the type of explosion, Type Ia or core collapse, that produced the explosion. Type Ia and ccSNe remnants can be distinguished by their degree of symmetry (e.g., Lopez et al. 2011), the relative abundance of iron and oxygen in the SNR (e.g., Vink 2012, Katsuda et al. 2018), or by the local stellar population (e.g., Badenes et al. 2009, Jennings et al. 2012, Auchettl et al. 2018). However, there appears to be no broad survey attempting to classify the Galactic SNRs by SN type.

A more challenging problem is that the detectable life time of an SNR depends on the nature of the explosion (e.g., Truelove & McKee 1999, Patnaude et al. 2017, Sarbadhicary et al. 2017). This will be correlated with the explosion energy and ejected mass, and this depends in turn on the binary status of the progenitor, since mass transfer can modify the properties of the exploding star. This problem can probably only be explored by models combining the predicted properties of the explosions with models for the evolution of the SNRs. Given the large statistical uncertainties of our present analysis, this seems unlikely to be an important problem at present.

Finally, there is the problem of doing a complete survey for compact remnants in Galactic SNRs, both for the 26 SNRs in Appendix B and more generally. The primary problem is simply that at fainter flux levels there begin to be multiple X-ray sources projected on the remnant with too little flux to be well-characterized given the exposure times. Unbound NS can be identified using X-ray proper motions on decade time scales, since the motion is $\simeq 0''.2$ per decade for a typical 250 km/s NS velocity at a distance of 3 kpc (e.g., Holland-Ashford et al. 2017). Longer observations to obtain adequate X-ray spectra would also make it relatively easy to classify the candidates. *We did see a dangerous propensity in the literature to reject X-ray sources with optical emission as candidates – as should be clear from this paper, one should*

expect some NS to have optical counterparts that are simply a normal, non-interacting star in a surviving binary!

It does appear that surviving binaries, like unbound stellar companions (Renzo et al. 2018), generally have low (tens of km/s) transverse velocities and should be located close to the point of explosion. After $t = 1000t_3$ years, a star moving at $v = 10v_{10}$ km/s has moved only $0''.7t_3v_{10}d_3^{-1}$ for a distance of $d = 3000d_3$ kpc. In many cases, the biggest uncertainty in the location of a surviving binary will be the difficulty in determining the center of explosion from the SNR (see, e.g., Holland-Ashford et al. 2017) rather than the distance of the binary from the center. That the velocities are so low should also greatly simplify searches for unbound companions (e.g., Kochanek 2018, Boubert et al. 2017).

ACKNOWLEDGMENTS

CSK thanks J. Beacom, T. Holland-Ashford, L. Lopez, K. Stanek, M. Pinsonneault, and T. Thompson for discussions and comments. CSK is supported by NSF grants AST-1515876 and AST-1515927. K. Belczynski acknowledges support from the Polish National Science Centre (NCN) grants: 2015/19/B/ST9/01099 and 2013/10/M/ST9/00729.

APPENDIX A: SNRS WITH IDENTIFIED COMPACT OBJECTS

- G034.7–00.4 contains the radio pulsar PSR J1856+0113 (Wolszczan et al. 1991) which is not a known binary in the ATNF Pulsar Catalog, nor is it listed as having a proper motion measurement (Manchester et al. 2005). The absorption of $N(H) = 0.9$ to 1.7×10^{22} cm⁻² (Shelton et al. 2004) only marginally meets our selection criteria. For an estimated distance of 3.0 ± 0.3 kpc (Ranasinghe & Leahy 2018), the PanSTARRS extinction of $E(B - V) \simeq 1.5$ agrees with the $E(B - V) \simeq 1.5$ to 2.9 estimated from the X-ray absorption. There appear to be no directed optical or near-IR searches for the pulsar, but it has no counterpart in either PanSTARRS or UKIDSS. We adopted limits of $g > 23.3$, $r > 23.2$, $i > 23.1$, $z > 22.3$ and $y > 21.3$ mag for PanSTARRS, and $J > 19.8$, $H > 19.0$ and $K > 18.1$ mag for UKIDSS.

- G039.7–02.0 contains the interacting compact object binary SS 433 (for a review, see Margon 1984). The SNR was identified prior to the discovery of SS 433. The X-ray flux is of order 4×10^{-12} erg cm⁻² s⁻¹. Brinkmann et al. (1996) find $N(H) = (5.5 \pm 1.5) \times 10^{21}$ cm², corresponding to $E(B - V) \simeq 0.9 \pm 0.3$. Marshall et al. (2013) estimate that the distance is 4.5 ± 0.2 kpc, while Blundell & Bowler (2004) find 5.5 ± 0.2 kpc. Either estimate is consistent with the Gaia DR2 parallax of 0.2161 ± 0.0626 mas. The PanSTARRS extinction estimates extend only to ~ 3.7 kpc, where they reach $E(B - V) \simeq 1.7$ and Margon (1984) cites $E(B - V) \simeq 2.6$. The optical fluxes of $V \sim 14.2$ and $B \sim 16.3$ mag (e.g., Margon 1984) and the 2MASS fluxes of $J = 9.4$, $H = 8.7$ and $K_s = 8.2$ mag are all dominated by accretion luminosity. If we treat any of these fluxes as upper limits, we find that they allow essentially any stellar mass. In practice, the goal has been to identify some spectroscopic signatures of the companion, with Hillwig & Gies (2008) estimating that the

companion mass is $(12.3 \pm 3.3)M_\odot$. Lockman et al. (2007) estimate that SS 433 has a 3D peculiar velocity of ~ 35 km/s. Using 1660 Gaia DR2 stars with parallaxes within 1σ of SS 433 to define the local rest frame, SS 433's proper motions of $(-2.85 \pm 0.10, -4.57 \pm 0.10)$ mas/year are statistically consistent with the mean and dispersion of $(-1.80 \pm 2.29, -4.13 \pm 2.68)$ mas/year found for these nearby stars. Formally, we find a 2D transverse velocity of 25 ± 8 km/s relative to the mean motion of these stars.

- G065.7+01.2 contains the resolved pulsar wind nebula (PWN) DA 495 and a central object J1952.2+2925 with a thermal X-ray spectrum and an unabsorbed X-ray flux of order 10^{-12} erg cm⁻² s⁻¹ (Arzoumanian et al. 2004). Arzoumanian et al. (2008) find $N(H) \simeq (2 - 7) \times 10^{21}$ cm² corresponding to $E(B - V) \simeq 0.7 \pm 0.5$. The amount of absorption very roughly constrains the distance to be between 1 and 5 kpc (Karpova et al. 2016), which is consistent with the PanSTARRS dust models. There is a PanSTARRS/UKIDSS source within $1''.1$ of the X-ray position having magnitudes $g = 20.21 \pm 0.02$, $r = 19.05 \pm 0.01$, $i = 18.48 \pm 0.02$, $z = 18.19 \pm 0.02$, $y = 17.77 \pm 0.02$, $J = 16.54 \pm 0.01$, $H = 16.05 \pm 0.01$ and $K = 15.82 \pm 0.03$. We adopt these as the limiting magnitude for any counterpart to the X-ray source. We could find no estimates of the transverse velocity.

- G069.0+02.7 (CTB 80) is associated with the radio pulsar PSR B1951+32 (Kulkarni et al. 1988). It is not reported to be a binary pulsar in the ATNF Pulsar Catalog (Manchester et al. 2005). It has an X-ray flux of roughly 4×10^{-13} erg cm⁻² s⁻¹ and $N(H) \simeq 3.0 \times 10^{21}$ cm⁻², corresponding to $E(B - V) \simeq 0.5$ mag (Safi-Harb et al. 1995). Butler et al. (2002) identify two possible optical counterparts to the pulsar with F547M magnitudes of 24.26 ± 0.30 and 24.54 ± 0.12 mag. Improved astrometry by Moon et al. (2004) is only consistent with the brighter of these two candidates. The PanSTARRS dust maps give $E(B - V) = 0.73$ for a distance of 2.4 kpc, consistent with the estimate from $N(H)$. Koo et al. (1993) roughly estimate the distance to CTB 80 to be $d \simeq 2$ kpc, while Leahy & Ranasinghe (2012) estimate a distance of $1.5^{+0.6}_{-0.4}$ kpc. Kulkarni et al. (1988) estimate 1.4 kpc from the dispersion measure to the pulsar. Migliazzo et al. (2002) measure a proper motion of $(-11.5 \pm 3.1, -26.3 \pm 3.7)$ mas/year corresponding to 240 ± 40 km/s at a distance of 2 kpc.

- G078.2+02.1 is associated with the γ -ray pulsar PSR J2021+4026, which is not a known pulsar binary in the ATNF pulsar catalog (Manchester et al. 2005). The X-ray flux is of order 9×10^{-13} erg cm⁻² s⁻¹. Landecker et al. (1980) estimate a distance of 1.5 ± 0.5 kpc. The X-ray absorption implies $N(H) = 6.4^{+0.8}_{-1.8} \times 10^{21}$ cm² (Hui et al. 2015), corresponding to $E(B - V) = 1.1 \pm 0.2$, while the PanSTARRS estimates span $E(B - V) = 1.5$ to 1.6 over the estimated distance range. Weisskopf et al. (2006) and Trepl et al. (2010) found no optical counterpart to the pulsar. Stronger limits are set by the absence of a counterpart in IPHAS ($r > 21.2$, $i > 20.0$, Barentsen et al. 2014) and UKIDSS (Lucas et al. 2008). H band provides the strongest limit on the mass of any stellar counterpart. Based on the position of the NS relative to the center of the SNR, Hui et al. (2015) estimate a transverse velocity of ~ 550 km/s.

- G106.3+02.7 is associated with the radio pulsar PSR J2229+6114 (Halpern et al. 2001b), which is not

a known pulsar binary in the ATNF pulsar catalog (Manchester et al. 2005). The X-ray flux is $\sim 2 \times 10^{-12}$ erg cm $^{-2}$ s $^{-1}$. X-ray absorption estimates give $N(H) = (6.3 \pm 1.3) \times 10^{21}$ cm 2 (Halpern et al. 2001a), corresponding to $E(B - V) = 1.1 \pm 0.2$ mag. Based on the X-ray absorption, Halpern et al. (2001a) argue for a distance of ~ 3 kpc, and at this distance, PanSTARRS estimates a consistent extinction of $E(B - V) \simeq 1.0$ mag. Halpern et al. (2001b) obtain a flux limit of $R < 23$ mag for any optical counterpart. We could find no estimates of the transverse velocity.

- G109.1–01.0 is associated with AXP 1E 2259+586 (Gregory & Fahlman 1980). The X-ray flux is $\sim 2 \times 10^{-11}$ erg cm $^{-2}$ s $^{-1}$. X-ray absorption estimates give $N(H) = (0.93 \pm 0.04) \times 10^{22}$ cm 2 (Patel et al. 2001), corresponding to $E(B - V) = 1.60 \pm 0.07$. Verbiest et al. (2012) estimate a distance of 4.1 ± 0.7 kpc and the PanSTARRS extinction estimates for this distance are lower, at $E(B - V) \simeq 0.9$ to 1.0 . Hulleman et al. (2000) report optical detection limits of $R > 25.7$ and $I > 24.3$ while Hulleman et al. (2001) report $R > 26.4$, $I > 25.6$, $J > 23.8$ and $K_s = 21.7 \pm 0.2$ mag. The IR flux is variable and correlated with the X-ray flux (Tam et al. 2004), so the IR detection should be viewed as an upper limit on any stellar companion. Tendulkar et al. (2013) measure a proper motion of $(-6.4 \pm 0.6, -2.3 \pm 0.6)$ mas/year corresponding to a transverse velocity of 157 ± 17 km/s for a distance of 3.2 kpc.

- G111.7–02.1 (Cas A) is associated with the X-ray source CXOU J232327.9+584842 discovered in the Chandra Observatory’s first light observations (Tananbaum 1999). It has an unabsorbed X-ray flux of flux 2×10^{-12} erg cm $^{-2}$ s $^{-1}$ with $N(H) \simeq (0.5 - 1.5) \times 10^{22}$ cm 2 , corresponding to $E(B - V) \simeq 1.7 \pm 0.9$. Reed et al. (1995) find a distance of roughly 3.4 ± 0.3 kpc. The PanSTARRS extinction estimate at this distance is $E(B - V) \simeq 1.2$ mag. Fesen et al. (2006) find no counterpart to the X-ray source to (STIS/50CCD) $R > 28$, (F110W) $J > 26.2$ and (F160W) $H > 24.6$ mag. Note that Kochanek (2018) and later Kerzendorf et al. (2018) had previously concluded that Cas A was not a binary at the time of death, including becoming an unbound binary. The distance of the NS from the expansion center of the SNR implies a transverse velocity of $\simeq 330$ km/s for a distance of 3.4 kpc.

- G114.3+00.3 is associated with radio pulsar PSR B2334+61 (Dewey et al. 1985) and it is not a known pulsar binary in the ATNF pulsar catalog (Manchester et al. 2005). It has an X-ray flux of 7×10^{-14} erg cm $^{-2}$ s $^{-1}$, and X-ray absorption estimates give $N(H) = (0.2 - 1.0) \times 10^{22}$ cm 2 (McGowan et al. 2006), corresponding to $E(B - V) \simeq 1.0 \pm 0.7$. Following McGowan et al. (2006) we adopt a distance of 3.2 ± 1.7 kpc, and over this distance range the PanSTARRS extinction estimates run from $E(B - V) \simeq 0.5$ to 1.0 mag. There is no counterpart to the pulsar in PanSTARRS (Chambers et al. 2016), which implies upper limits of $g > 23.3$, $r > 23.2$, $i > 23.1$, $z > 22.3$ and $y > 21.3$ mag. The z band limit is the most constraining. Hobbs et al. (2004) measured a proper motion of $(-1 \pm 18, -15 \pm 16)$ mas/year. For 1705 stars with parallaxes consistent with this distance estimate, we find a mean and dispersion in the proper motions of $(-2.15 \pm 2.40, -1.10 \pm 1.60)$ mas/year. This leads to a weak estimate of the transverse velocity of 212 ± 268 km/s.

Boubert et al. (2017) identify TYC 4280-562-1 in this SNR as a candidate, disrupted binary star.

- G119.5+10.2 (CTA 1) is associated with the X-ray source RX J0007.0+7303 (Halpern et al. 2004) which was later found to be a γ -ray (Abdo et al. 2008) and X-ray (Lin et al. 2010) pulsar. The X-ray flux is 2×10^{-13} erg cm $^{-2}$ s $^{-1}$. Pineault et al. (1993) estimate a distance of 1.4 ± 0.3 kpc. Slane et al. (1997) find $N(H) = 2.8_{-0.5}^{+0.6} \times 10^{21}$ cm 2 implying $E(B - V) \simeq 0.5 \pm 0.1$, consistent with the PanSTARRS estimate of $E(B - V) \simeq 0.3$. Mignani et al. (2013) obtained optical limits on any counterpart to the X-ray source of $V > 26.9$ and $r > 27.6$ mag. Slane et al. (2004a) estimated a transverse velocity of ~ 450 km/s for a distance of 1.4 kpc based on the offset of the NS from the geometric center of the SNR.

- G130.7+03.1 (3C58, SN 1181) is associated with the X-ray pulsar PSR J0205+6449 (Murray et al. 2002). The X-ray flux is 9×10^{-13} erg cm $^{-2}$ s $^{-1}$. Slane et al. (2004b) find $N(H) = (4.5 \pm 0.1) \times 10^{21}$ cm 2 , corresponding to $E(B - V) \simeq 0.77 \pm 0.02$, while the PanSTARRS estimates are $E(B - V) \simeq 0.5$ to 0.7 . Roberts et al. (1993) estimate a kinematic (HI) distance of 3.2 kpc, while Camilo et al. (2002b) obtain $4.5_{-1.2}^{+1.6}$ kpc based on the dispersion measure to the pulsar. Moran et al. (2013) report optical detections of $g \simeq 27.4 \pm 0.2$, $r \simeq 26.2 \pm 0.3$ and $i \simeq 25.5 \pm 0.2$ mag but interpret it as emission from the pulsar. Bietenholz et al. (2013) measure a proper motion of $(-1.40 \pm 0.16, 0.54 \pm 0.58)$ mas/year. Based on 1612 stars having parallaxes consistent with the compact object, we find a mean and dispersion in the proper motions of $(-0.71 \pm 1.79, 0.17 \pm 1.39)$ mas/year. This is very similar to the proper motion of the pulsar, leading to a transverse velocity of 17 ± 9 km/s that is somewhat lower than the estimate of 35 ± 6 km/s from Bietenholz et al. (2013). The pulsar does lie close to the center of the SNR, as would be expected for such a low transverse velocity.

- G180.0–01.7 is associated with the radio pulsar PSR J0538+2817 (Anderson et al. 1996) and it is not a known pulsar binary in the ATNF pulsar catalog (Manchester et al. 2005). The X-ray flux is 1.7×10^{-12} erg cm $^{-2}$ s $^{-1}$. The VLBI parallax (0.68 ± 0.15 mas) distance to the pulsar is $1.5_{-0.3}^{+0.4}$ kpc (Ng et al. 2007). Ng et al. (2007) also find $N(H) \simeq (2.7 \pm 0.3) \times 10^{21}$ cm 2 , implying $E(B - V) \simeq 0.5 \pm 0.1$, a little lower than the PanSTARRS estimate of $E(B - V) \simeq 0.65$. There is no PanSTARRS counterpart to the pulsar. Ng et al. (2007) measure a proper motion of $(-23.53 \pm 0.16, 52.59 \pm 0.13)$ mas/year. Based on 1573 stars with parallaxes consistent with the compact object, we find a mean and dispersion in the proper motions of $(1.04 \pm 2.57, -2.86 \pm 3.29)$ mas/year. This implies a transverse velocity of 425 ± 94 km/s, consistent the Ng et al. (2007) estimate of 400_{-73}^{+114} km/s. This is the SNR where Dinçel et al. (2015) and Boubert et al. (2017) identify HD 37424 as a candidate disrupted binary companion.

- G184.6–05.8 (Crab, SN 1054) is associated with the Crab radio pulsar PSR B0531+21 (Staelin & Reifenstein 1968), which is not a known pulsar binary (Manchester et al. 2005). Willingale et al. (2001) find $N(H) = (3.45 \pm 0.02) \times 10^{21}$ cm 2 , corresponding to $E(B - V) \simeq 0.587 \pm 0.003$ in reasonable agreement with the PanSTARRS estimate of $E(B - V) \simeq 0.4$. We adopt a distance of 2.0 ± 0.5 kpc (Kaplan et al. 2008). Sandberg & Sollerman (2009) give magnitudes of

$V = 16.66 \pm 0.03$, $R = 16.17 \pm 0.02$, $I = 15.65 \pm 0.02$, $z = 15.39 \pm 0.05$, $J = 14.83 \pm 0.03$, $H = 14.28 \pm 0.02$ and $K_s = 13.80 \pm 0.01$ mag. This is all non-thermal emission from the pulsar (see the review of the Crab by Hester 2008), and non-detection of a binary in the pulsar timing represents a much stronger mass limit on any companion. In the local standard of rest of the Crab, Kaplan et al. (2008) estimate that the proper motions are $(-11.8 \pm 2.0, 4.4 \pm 2.0)$ mas/year, corresponding to a transverse velocity of 120 km/s at a distance of 2 kpc.

- G189.1+03.0 (IC 443) is associated with the NS CXO J061705.3+222127 and the PWN G189.22+2.90 (Keohane et al. 1997). The total (PWN+NS) X-ray flux is 5×10^{-12} erg cm $^{-2}$ s $^{-1}$. Fesen (1984) estimates a distance to the remnant of 1.5 to 2.0 kpc, which is supported by Welsh & Sallmen (2003). Gaensler et al. (2006) find $N(H) = (7.2 \pm 0.6) \times 10^{21}$ cm 2 , corresponding to $E(B - V) \simeq 1.2 \pm 0.1$, while the PanSTARRS estimates for the assumed distances are lower at $E(B - V) \simeq 0.8$. There is no PanSTARRS source corresponding to the X-ray source. Swartz et al. (2015) estimate a transverse velocity of 400-600 km/s based on the separation of the NS from the geometric center of the SNR for a distance of 1.5 kpc.

- G205.5+00.5 (Monoceros Loop) is associated with the γ -ray source HESS J0632+057. The SNR was identified prior to the discovery of the γ -ray source. Hinton et al. (2009) also identified it as an X-ray source and suggested that it was in a binary with the massive star MWC 148. The high energy emissions are believed to be due to interactions between a pulsar and the stellar wind (see the review by Dubus 2013). Hinton et al. (2009) find $N(H) = (3.1 \pm 0.3) \times 10^{21}$ cm 2 corresponding to $E(B - V) \simeq 0.53 \pm 0.05$. Odegard (1986) estimated an HI distance of 1.6 kpc while Zhao et al. (2018) find 2.0 kpc. The PanSTARRS extinction estimate for these distances is $E(B - V) \simeq 0.6$. MWC 148 has a Gaia DR2 parallax of 0.3625 ± 0.0440 mas that is consistent with the SNR distance estimates. The star has 2MASS magnitudes of $J = 7.64 \pm 0.02$, $H = 7.39 \pm 0.05$ and $K_s = 6.97 \pm 0.02$, APASS magnitudes of $V = 9.07$, $B = 9.63$, $g = 9.34$, $r = 8.78$ and $i = 8.70$ mag, and Neckel et al. (1980) find $V = 9.17$, $B = 9.72$, and $U = 9.17$. Bongiorno et al. (2011) found a 321 ± 5 day periodicity in the X-ray emission, a period consistent with the radial velocity variations of the star (Casares et al. 2012, Moritani et al. 2018). Aragona et al. (2010) obtain a spectroscopic temperature of $\log T \simeq 30000$ K and combining this with SED fits estimate that the mass of the star is $13M_{\odot} < M < 19M_{\odot}$. When we fit these magnitudes to the PARSEC models, using the average B and V magnitudes, the priors in Table 2, uncertainties of 0.1 mag, and terms for the Gaia parallax and the spectroscopic temperature ($T = 29000 \pm 2000$ K) we find a best fit model with $M = 29M_{\odot}$ ($20M_{\odot} < M < 36M_{\odot}$, for $\Delta\chi^2 = 4$), $T \simeq 29200$ K ($24100 < T < 32100$), $d \simeq 2.26$ kpc ($1.97 < d < 2.58$), and $E(B - V) \simeq 0.96$ ($0.92 < E(B - V) < 0.98$). The fits are not great ($\chi^2 = 34$), presumably because we have not taken into account any emission from the disk of this B0pe star (see Aragona et al. 2010), but are broadly consistent with the prior estimates. Using 1260 stars having parallaxes consistent with MWC 148 to define a local rest frame, we find a 2D transverse velocity of 3 ± 1 km/s. The proper motion of MWC 148, $(-0.08 \pm 0.08, -0.55 \pm 0.07)$ mas/year is

statistically consistent with the local mean and dispersion of $(-0.05 \pm 1.78, -0.80 \pm 2.18)$ mas/year. Boubert et al. (2017) identify HD 261393 as a candidate disrupted binary companion in this SNR. However, it was identified by only one of their two methods, and the existence of the HMXB makes the identification unlikely.

- G260.4–03.4 (Puppis A) was first associated with an X-ray source (Petre et al. 1996) that was later found to be an X-ray pulsar (PSR J0821–4300, Gotthelf & Halpern 2009). It has an X-ray flux of 3×10^{-12} erg cm $^{-2}$ s $^{-1}$. Reynoso et al. (2017) estimate a kinematic distance to the SNR of 1.3 ± 0.3 kpc. Hui & Becker (2006) find $N(H) = (3.7 \pm 0.1) \times 10^{21}$ cm 2 corresponding to $E(B - V) = 0.63 \pm 0.02$. This cannot be checked in PanSTARRS as it lies outside of the PS1 survey region. Mignani et al. (2009) find no optical counterpart down to 5σ limits of $B \simeq 27.2$, $V \simeq 26.9$ and $I \simeq 25.6$ mag. Becker et al. (2012) measure a proper motion of $(-64 \pm 12, -31 \pm 13)$ mas/year. Based on 1857 stars having parallaxes consistent with the compact object, we find a mean and dispersion in the proper motions of $(-3.32 \pm 2.94, 4.00 \pm 3.58)$ mas/year. This implies a transverse velocity of 433 ± 126 km/s. This is lower than the estimate of 672 ± 115 km/s by Becker et al. (2012) only because they use a larger distance of 2 kpc.

- G263.9–03.3 (Vela) is associated with the Vela pulsar (PSR J0835–4510, Large et al. 1968). The PWN has an X-ray flux of 5×10^{-11} erg cm $^{-2}$ s $^{-1}$, and Pavlov et al. (2001a) find $N(H) = (3.0 \pm 0.3) \times 10^{20}$ cm 2 , implying a negligible extinction of $E(B - V) \simeq 0.05$. The VLBI parallax distance to the pulsar is 0.29 ± 0.02 kpc (Dodson et al. 2003). Nasuti et al. (1997) measured optical fluxes of $U = 23.38 \pm 0.15$, $B = 23.89 \pm 0.15$, $V = 23.65 \pm 0.10$ and $R = 23.93 \pm 0.20$ which is believed to be emission from the pulsar. Dodson et al. (2003) measure a proper motion of $(-49.68 \pm 0.06, 29.9 \pm 0.1)$ mas/year. Based on 1414 stars having parallaxes consistent with the compact object, we find a mean and dispersion in the proper motions of $(-5.46 \pm 10.18, 3.93 \pm 11.65)$ mas/year. This implies a transverse velocity of 70 ± 8 km/s, consistent with the estimate of 62 ± 2 km/s by Dodson et al. (2003), where their smaller uncertainty does not include a contribution from the kinematic model.

- G266.2–01.2 (Vela Jr.) is associated with the X-ray source CXOU J085201.4–461753 (Pavlov et al. 2001b). It has a flux of 2×10^{-12} erg cm $^{-2}$ s $^{-1}$, and Pavlov et al. (2001b) find $N(H) = (3 \pm 1) \times 10^{21}$ cm 2 corresponding to $E(B - V) \simeq 0.5 \pm 0.2$. Allen et al. (2015) adopt a distance of 0.7 ± 0.2 kpc. Mignani et al. (2007b) identify a possible counterpart in the near-IR with $R > 25.6$, $J > 22.6$, $H \simeq 21.6 \pm 0.1$ and $K_s \simeq 21.4 \pm 0.2$ mag. We could find no estimates of the transverse velocity.

- G284.3–01.8 is associated with the γ -ray source 1FGL J1018.6-5856, and it was identified as an HMXB by Corbet et al. (2011). There is also an X-ray pulsar, PSR J1016–5857, on the edge or just outside the remnant (Camilo et al. 2001), which we will ignore. The SNR was identified prior to the discovery of the binary. Like HESS J0632+057, the high energy emission is believed to be due to interactions between a pulsar and the stellar wind (see the review by Dubus 2013). The binary has an X-ray flux of 2×10^{-12} erg cm $^{-2}$ s $^{-1}$. Williams et al. (2015) find $N(H) = (9.0 \pm 0.9) \times 10^{21}$ cm 2 , corresponding to

$E(B - V) \simeq 1.5 \pm 0.2$. The Gaia DR2 parallax is 0.153 ± 0.025 mas, consistent with the previous distance estimate of $5.4_{-2.1}^{+4.6}$ kpc by Napoli et al. (2011). The star is a main sequence O6 star (Corbet et al. 2011, Waisberg & Romani 2015), and Napoli et al. (2011) successfully model the spectral energy distribution with $R = 10.1R_{\odot}$, $T = 38900$ K, $L = 10^{5.3}L_{\odot}$ for $E(B - V) = 1.34$ and $d = 5.4$ kpc. Both Waisberg & Romani (2015) and Strader et al. (2015) favor a NS as the compact companion. The binary period is 16.6 days (Fermi LAT Collaboration et al. 2012). The 2MASS magnitudes are $J = 10.44$, $H = 10.14$ and $K_s = 10.02$ and the AAVSO magnitudes are $B = 13.64$, $V = 12.68$, $g = 13.16$, $r = 12.29$, and $i = 11.85$. We fit these magnitudes assuming 0.1 mag uncertainties with the distance and extinction priors from Table 2 and then added terms for the Gaia DR2 parallax and the spectroscopic temperature ($T = 38000 \pm 2000$ K for O6, Martins et al. 2005) to the goodness of fit. This leads to a mass estimate of $40M_{\odot}$ ($29M_{\odot} < M < 61M_{\odot}$) with distances and extinctions of $5.0 < d < 9.2$ kpc and $1.33 < E(B - V) < 1.35$, respectively, consistent with Napoli et al. (2011). If we include the Swift photometry from Fermi LAT Collaboration et al. (2012), we are unable to obtain a good fit to the SED ($\chi^2 = 356$ instead of 2.8), but the best models favor lower masses, temperatures and extinctions ($M \simeq 20M_{\odot}$, $T \simeq 10^4$ K, $E(B - V) \simeq 1.0$). Using 1562 stars with consistent parallaxes, we estimate a transverse velocity of 39 ± 7 km/s. The proper motion of the binary, $(-6.41 \pm 0.05, 2.21 \pm 0.05)$ mas/year, is statistically consistent with the motions of nearby stars, which have a mean and dispersion of $(-5.51 \pm 1.91, 3.10 \pm 1.67)$ mas/year.

- G291.0–00.1 is associated with the PSR candidate CXOU J111148.6–603926 and a PWN with an X-ray flux of 4×10^{-13} erg cm $^{-2}$ s $^{-1}$ (Slane et al. 2012). Slane et al. (2012) find $N(H) = (6.7 \pm 0.7) \times 10^{21}$ cm 2 , corresponding to $E(B - V) \simeq 1.1 \pm 0.1$. The distance to the SNR is not well established, with a minimum distance of 3.5 kpc and a typical scaling to 5 kpc (see the discussion in Slane et al. 2012). There is no optical counterpart in Gaia DR2, which we interpret at $G < 22$, $G_{BP} < 20$ and $G_{RP} < 20$ mag. Holland-Ashford et al. (2017) used proper motions to derive a transverse velocity of 303 ± 130 km/s for a distance of 5 kpc.

- G296.5+10.0 is associated with the X-ray PSR J1210–5226 (Zavlin et al. 2000). It has an X-ray flux of 2×10^{-12} erg cm $^{-2}$ s $^{-1}$, and de Luca et al. (2004) find $N(H) = (1.3 \pm 0.1) \times 10^{21}$ cm 2 , corresponding to $E(B - V) \simeq 0.22 \pm 0.02$. Giacani et al. (2000) estimate a distance of $2.1_{-0.8}^{+1.8}$ kpc. de Luca et al. (2004) also found no optical counterparts down to $R > 27.1$ and $V > 27.3$ mag. We could find no estimates of the transverse velocity.

- G320.4–01.2 is associated with the X-ray pulsar PSR J1513–5908 (Seward & Harnden 1982). The X-ray flux is 6×10^{-12} erg cm $^{-2}$ s $^{-1}$, and Yatsu et al. (2005) find $N(H) = (0.86 \pm 0.09) \times 10^{22}$ cm 2 , corresponding to $E(B - V) \simeq 1.5 \pm 0.2$ which cannot be checked with PanSTARRS. Gaensler et al. (1999) estimate a distance of 5.2 ± 1.4 kpc. Kaplan et al. (2006a) identify a possible counterpart with $R \simeq 25.6 \pm 0.3$, $J > 20.7$, $H \simeq 20.6 \pm 0.2$ and $K_s \simeq 19.4 \pm 0.1$ mag, but argue that the emission is likely from the pulsar. We could find no estimates of the transverse velocity.

- G332.4–00.4 contains the central compact object

1E 161348–5055 (Tuohy & Garmire 1980). The X-ray flux shows a $\simeq 6.7$ hour periodicity. Reynoso et al. (2004) estimate a distance of 3.1 kpc, and Frank et al. (2015) find column densities of $N(H) = (0.6 - 1.4) \times 10^{22}$ cm $^{-2}$ corresponding to $E(B - V) \simeq 1.0$ to 2.4. The field is crowded, and De Luca et al. (2008) find no compelling near-IR counterpart to the X-ray source. If we use their near-IR limits of $H > 23$ and $K_s > 22.1$ mag, then the mass limit is $< 0.1M_{\odot}$. If we identify the counterpart as their star #5 with $H = 21.43 \pm 0.01$ and $K = 19.22 \pm 0.21$, then the limit is $< 0.2M_{\odot}$. However, De Luca et al. (2008) note that the colors of star #5 are those of a more distant, more heavily extincted source. We treat this as a non-detection.

APPENDIX B: SNRS WITHOUT IDENTIFIED COMPACT OBJECTS

- G007.7–03.7 has no reported association, although there are X-ray observations of the remnant (Zhou et al. 2018).

- G025.1–02.3 has no reported association. It is not clear whether it has ever been searched for either an X-ray source or a radio pulsar.

- G032.8–00.1 has an unrelated pulsar, PSR J1853–0004, and an unrelated background variable X-ray source (2XMM J185114.3–000004, Bamba et al. 2016).

- G038.7–01.3 contains four faint X-ray sources (Huang et al. 2014) but they are all below our flux limit of 10^{-13} erg cm $^{-2}$ s $^{-1}$.

- G053.6–02.2 has no associated sources, but has been observed in X-rays (e.g., Broersen & Vink 2015).

- G055.7+3.4 meets our selection criteria, but is little studied. The pulsar PSR J1921+2153 lies on the edge of the shell and is probably unrelated (Bhatnagar et al. 2011).

- G065.3+05.7 meets our selection criteria. The pulsar PSR J1931+30 is nearby, but probably is not associated. No candidate NS has been identified in X-ray observations (Kaplan et al. 2006a).

- G074.0–08.5 (Cygnus Loop) contains a 2×10^{-13} erg cm $^{-2}$ s $^{-1}$ X-ray source, but its properties make it unlikely to be associated with the SNR unless it has a very high (~ 2000 km/s) transverse velocity (Katsuda et al. 2012).

- G082.2+05.3 has no associated sources, but has been observed in X-rays (e.g., Mavromatakis et al. 2004).

- G085.4+00.7 has a number of superposed X-ray sources (Jackson et al. 2008), some of which may slightly exceed our 10^{-13} erg cm $^{-2}$ s $^{-1}$ flux limit (the paper does not report fluxes). None are identified as a likely NS.

- G085.9–00.6 has a number of superposed X-ray sources (Jackson et al. 2008), some of which may slightly exceed our 10^{-13} erg cm $^{-2}$ s $^{-1}$ flux limit (the paper does not report fluxes). None are identified as a likely NS. ‘

- G089.0+04.7 has X-ray observations (e.g., Pannuti et al. 2010), but no reported association.

- G093.3+06.9 contains a candidate PWN, but the flux is only 4×10^{-14} erg cm $^{-2}$ s $^{-1}$ (Jiang et al. 2007).

- G116.9+00.2 (CTB 1) has been associated with the X-ray source RX J0002+6246, with an X-ray flux of 3×10^{-13} erg cm $^{-2}$ s $^{-1}$. However, Esposito et al. (2008) con-

clude that it is actually X-ray emission from a foreground star. The Gaia DR2 parallax of the star, 3.137 ± 0.038 mas, confirms this conclusion.

- G127.1+00.5 has no X-ray sources brighter than 5×10^{-14} erg cm $^{-2}$ s $^{-1}$ and this source has the X-ray/optical flux ratio of a star (Kaplan et al. 2004).

- G132.7+01.3 (HB3) is near the radio pulsar PSR J0215+6218. However, Lorimer et al. (1998) do not believe the two are associated because the spin down age is orders of magnitude larger than the estimated age of the SNR.

- G156.2+05.7 has no associated X-ray source (Kaplan et al. 2006a).

- G160.9+02.6 (HB9) is unlikely to be associated with SGR 0501+4516, as it lies outside the rim of the SNR (e.g., Gaensler & Chatterjee 2008). The SNR is also probably unrelated to PSR B0459+47/J0502+4654/B0458+46 (see, e.g., Kaplan et al. 2006a).

- G166.0+04.3 has X-ray observations (e.g., Bocchino et al. 2009), but no associated source.

- G296.1–00.5 has X-ray observations (e.g., Castro et al. 2011), but no associated source.

- G309.2–00.6 contains an X-ray source, but it is an unrelated, foreground Be star (Safi-Harb et al. 2007).

- G326.3–01.8 is associated with an X-ray point source/PWN with a flux of 5×10^{-14} erg cm $^{-2}$ s $^{-1}$ (Yatsu et al. 2013), which is below our flux threshold.

- G330.0+15.0 (Lupus loop) has no X-ray sources above $\sim 1 \times 10^{-13}$ erg cm $^{-2}$ s $^{-1}$ (Kaplan et al. 2006a).

- G332.5–05.6 has no associated source.

- G343.1–02.3 is associated with the radio pulsar PSR J1709–4429 (Johnston et al. 1992), but it lies near the very edge of the remnant. It is difficult to reconcile its properties with the transverse velocity required to reach the edge of the SNR (see the discussions in Dodson & Golap 2002 and Romani et al. 2005). The X-ray flux is 2×10^{-13} erg cm $^{-2}$ s $^{-1}$.

- G343.0–0.60 has no associated source.

APPENDIX C: REJECTED SNRS

- G004.5+06.8 (Kepler) is a Type Ia SN (e.g., Reynolds et al. 2007).

- G011.1+00.1 is probably a remnant in the background of the closer PSR J1809–1917 (see Kargaltsev & Pavlov 2007). The Manitoba SNR catalog uses the distance to the pulsar, but our distance selection criterion is meant to apply to the SNR. Hence, neither the compact object nor the SNR should be included in our statistics.

- G120.1+01.4 (Tycho) is a Type Ia SN (e.g., Krause et al. 2008).

- G315.4–02.3 is generally identified as a Type Ia remnant (e.g., Williams et al. 2011, Yamaguchi et al. 2014). In particular, the Fe K α line emission of the remnant is typical of Type Ia SNRs and incompatible with that of core collapse SNRs (Yamaguchi et al. 2014). The distance is 2.5 ± 0.5 kpc (Helder et al. 2013) and Castro et al. (2013) find $N(H) = 6 \times 10^{21}$ cm $^{-2}$ corresponding to $E(B - V) \simeq 1.0$. Gvaramadze et al. (2017) propose that the X-ray source identified as [GV2003]N in Gvaramadze & Vikhlinin (2003) is a surviving low mass NS binary associated with a core col-

lapse SNe that produces the SNR despite lying at the remnant edge. The source has $V = 20.69 \pm 0.02$, $i = 18.77 \pm 0.08$, $z = 18.29 \pm 0.06$, $J = 16.71 \pm 0.17$, $H = 15.87 \pm 0.14$, $K_s = 15.73 \pm 0.18$ Vega mag and a spectroscopic temperature of $T_* = 5100 \pm 200$ K. With our standard fitting procedures, we find reasonably good fits for a $0.9M_\odot < M_* < 1.2M_\odot$ main sequence star, consistent with the estimate by Gvaramadze et al. (2017). The abundances of this G star appears to be anomalous, which Gvaramadze et al. (2017) interpret as contamination by ejecta from a calcium-rich SN. It is also difficult to reconcile the typical distance of Ca-rich SN from their host galaxies (e.g., Kasliwal et al. 2012) with a massive star origin for the Ca-rich transients. Unfortunately, the Gaia DR2 parallax of the source ($\pi = 8.0 \pm 1.0$ mas, or a distance of 125 ± 15 kpc) seems to be clearly wrong since it also has a fit statistic of $\chi^2 = 2392$. In our view, this binary seems most likely to be a chance projection.

- G327.6+14.6 is the remnant of SN 1006, which was probably a Type Ia SN (see the review by Vink 2012).

REFERENCES

- Abbott, B. P., Abbott, R., Abbott, T. D., et al. 2016, *Physical Review Letters*, 116, 061102
- Abbott, B. P., Abbott, R., Abbott, T. D., et al. 2017, *Physical Review Letters*, 119, 161101
- Abdo, A. A., Ackermann, M., Atwood, W. B., et al. 2008, *Science*, 322, 1218
- Abdo, A. A., Ackermann, M., Ajello, M., et al. 2009, *Science*, 325, 840
- Allen, G. E., Chow, K., DeLaney, T., et al. 2015, *ApJ*, 798, 82
- Anderson, S. B., Cadwell, B. J., Jacoby, B. A., et al. 1996, *ApJL*, 468, L55
- Aragona, C., McSwain, M. V., & De Becker, M. 2010, *ApJ*, 724, 306
- Arzoumanian, Z., Safi-Harb, S., Landecker, T. L., & Kothes, R. 2004, *ApJL*, 610, L101
- Arzoumanian, Z., Safi-Harb, S., Landecker, T. L., Kothes, R., & Camilo, F. 2008, *ApJ*, 687, 505-515
- Arzoumanian, Z., Gotthelf, E. V., Ransom, S. M., et al. 2011, *ApJ*, 739, 39
- Auchettl, K., Lopez, L., Badenes, C., et al. 2018, *arXiv:1804.10210*
- Badenes, C., Harris, J., Zaritsky, D., & Prieto, J. L. 2009, *ApJ*, 700, 727
- Bamba, A., Terada, Y., Hewitt, J., et al. 2016, *ApJ*, 818, 63
- Barentsen, G., Farnhill, H. J., Drew, J. E., et al. 2014, *MNRAS*, 444, 3230
- Becker, W., Prinz, T., Winkler, P. F., & Petre, R. 2012, *ApJ*, 755, 141
- Belczynski, K., Kalogera, V., & Bulik, T. 2002, *ApJ*, 572, 407
- Belczynski, K., Kalogera, V., Rasio, F. A., et al. 2008, *ApJS*, 174, 223
- Belczynski, K., Wiktorowicz, G., Fryer, C. L., Holz, D. E., & Kalogera, V. 2012, *ApJ*, 757, 91
- Belczynski, K., Heger, A., Gladysz, W., et al. 2016, *AAP*, 594, A97

- Belczynski, K., Klencki, J., Meynet, G., et al. 2017, arXiv:1706.07053
- Bersten, M. C., Benvenuto, O. G., Folatelli, G., et al. 2014, *AJ*, 148, 68
- Bhatnagar, S., Rau, U., Green, D. A., & Rupen, M. P. 2011, *ApJL*, 739, L20
- Bietenholz, M. F., Kondratiev, V., Ransom, S., et al. 2013, *MNRAS*, 431, 2590
- Binney, J., & Merrifield, M. 1998, *Galactic astronomy / James Binney and Michael Merrifield*. Princeton, NJ : Princeton University Press, 1998. (Princeton series in astrophysics) QB857 .B522 1998
- Blaauw, A. 1961, *BAIN*, 15, 265
- Bocchino, F., Miceli, M., & Troja, E. 2009, *AAP*, 498, 139
- Boubert, D., Fraser, M., Evans, N. W., Green, D. A., & Izzard, R. G. 2017, *AAP*, 606, A14
- Blundell, K. M., & Bowler, M. G. 2004, *ApJL*, 616, L159
- Bohlin, R. C., Savage, B. D., & Drake, J. F. 1978, *ApJ*, 224, 132
- Bongiorno, S. D., Falcone, A. D., Stroh, M., et al. 2011, *ApJL*, 737, L11
- Brinkmann, W., Aschenbach, B., & Kawai, N. 1996, *AAP*, 312, 306
- Broersen, S., & Vink, J. 2015, *MNRAS*, 446, 3885
- Butler, R. F., Golden, A., & Shearer, A. 2002, *AAP*, 395, 845
- Camilo, F., Bell, J. F., Manchester, R. N., et al. 2001, *ApJL*, 557, L51
- Camilo, F., Manchester, R. N., Gaensler, B. M., Lorimer, D. R., & Sarkissian, J. 2002a, *ApJL*, 567, L71
- Camilo, F., Stairs, I. H., Lorimer, D. R., et al. 2002b, *ApJL*, 571, L41
- Cardelli, J. A., Clayton, G. C., & Mathis, J. S. 1989, *ApJ*, 345, 245
- Castro, D., Slane, P. O., Gaensler, B. M., Hughes, J. P., & Patnaude, D. J. 2011, *ApJ*, 734, 86
- Castro, D., Lopez, L. A., Slane, P. O., et al. 2013, *ApJ*, 779, 49
- Caswell, J. L., McClure-Griffiths, N. M., & Cheung, M. C. M. 2004, *MNRAS*, 352, 1405
- Casares, J., Ribó, M., Ribas, I., et al. 2012, *MNRAS*, 421, 1103
- Chambers, K. C., Magnier, E. A., Metcalfe, N., et al. 2016, arXiv:1612.05560
- Chen, Y., Bressan, A., Girardi, L., et al. 2015, *MNRAS*, 452, 1068
- Chevalier, C., & Ilovaisky, S. A. 1998, *AAP*, 330, 201
- Coe, M. J. 2005, *MNRAS*, 358, 1379
- Corbet, R. H. D., Cheung, C. C., Kerr, M., et al. 2011, *The Astronomer's Telegram*, 3221,
- Cordes, J. M., & Chernoff, D. F. 1998, *ApJ*, 505, 315
- Cordes, J. M., & Lazio, T. J. W. 2002, arXiv:astro-ph/0207156
- Crawford, F., Gaensler, B. M., Kaspi, V. M., et al. 2001, *ApJ*, 554, 152
- de Luca, A., Mereghetti, S., Caraveo, P. A., et al. 2004, *AAP*, 418, 625
- De Luca, A., Mignani, R. P., Zaggia, S., et al. 2008, *ApJ*, 682, 1185
- de Luca, A., Caraveo, P. A., Esposito, P., & Hurley, K. 2009, *ApJ*, 692, 158
- de Mink, S. E., & Belczynski, K. 2015, *ApJ*, 814, 58
- Dessart, L., Burrows, A., Ott, C. D., et al. 2006, *ApJ*, 644, 1063
- Dewey, R. J., Taylor, J. H., Weisberg, J. M., & Stokes, G. H. 1985, *ApJL*, 294, L25
- Diñçel, B., Neuhäuser, R., Yerli, S. K., et al. 2015, *MNRAS*, 448, 3196
- Dodson, R., & Golap, K. 2002, *MNRAS*, 334, L1
- Dodson, R., Legge, D., Reynolds, J. E., & McCulloch, P. M. 2003, *ApJ*, 596, 1137
- Dominik, M., Belczynski, K., Fryer, C., et al. 2012, *ApJ*, 759, 52
- Dubus, G. 2013, *A&ARv*, 21, 64
- Duchêne, G., & Kraus, A. 2013, *ARA&A*, 51, 269
- Eldridge, J. J., Izzard, R. G., & Tout, C. A. 2008, *MNRAS*, 384, 1109
- Esposito, P., de Luca, A., Tiengo, A., et al. 2008, *MNRAS*, 384, 225
- Faucher-Giguère, C.-A., & Kaspi, V. M. 2006, *ApJ*, 643, 332
- Fermi LAT Collaboration, Ackermann, M., Ajello, M., et al. 2012, *Science*, 335, 189
- Ferrand, G., & Safi-Harb, S. 2012, *Advances in Space Research*, 49, 1313
- Fesen, R. A. 1984, *ApJ*, 281, 658
- Fesen, R. A., Pavlov, G. G., & Sanwal, D. 2006, *ApJ*, 636, 848
- Folatelli, G., Bersten, M. C., Benvenuto, O. G., et al. 2014, *ApJL*, 793, L22
- Fox, O. D., Azalee Bostroem, K., Van Dyk, S. D., et al. 2014, *ApJ*, 790, 17
- Frank, K. A., Burrows, D. N., & Park, S. 2015, *ApJ*, 810, 113
- Fryer, C. L., Belczynski, K., Wiktorowicz, G., et al. 2012, *ApJ*, 749, 91
- Gaensler, B. M., Brazier, K. T. S., Manchester, R. N., Johnston, S., & Green, A. J. 1999, *MNRAS*, 305, 724
- Gaensler, B. M., & Wallace, B. J. 2003, *ApJ*, 594, 326
- Gaensler, B. M., Chatterjee, S., Slane, P. O., et al. 2006, *ApJ*, 648, 1037
- Gaensler, B. M., & Chatterjee, S. 2008, *GRB Coordinates Network*, 8149, 1
- Gaia Collaboration, Brown, A. G. A., Vallenari, A., et al. 2018, arXiv:1804.09365
- Gvaramadze, V. V., & Vikhlinin, A. A. 2003, *AAP*, 401, 625
- Gvaramadze, V. V., Langer, N., Fossati, L., et al. 2017, *Nature Astronomy*, 1, 0116
- Giacani, E. B., Dubner, G. M., Green, A. J., Goss, W. M., & Gaensler, B. M. 2000, *AJ*, 119, 281
- Gies, D. R., & Bolton, C. T. 1986, *ApJS*, 61, 419
- González Hernández, J. I., Reboló, R., Peñarrubia, J., Casares, J., & Israelian, G. 2005, *AAP*, 435, 1185
- González Hernández, J. I., Ruiz-Lapuente, P., Tabernero, H. M., et al. 2012, *Nature*, 489, 533
- Gotthelf, E. V., & Halpern, J. P. 2009, *ApJL*, 695, L35
- Green, D. A. 2014, *Bulletin of the Astronomical Society of India*, 42, 47
- Green, G. M., Schlafly, E. F., Finkbeiner, D. P., et al. 2015, *ApJ*, 810, 25
- Gregory, P. C., & Fahlman, G. G. 1980, *Nature*, 287, 805
- Gunn, J. E., & Ostriker, J. P. 1970, *ApJ*, 160, 979
- Guseinov, O. H., Ankay, A., & Tagieva, S. O. 2005, *Astro-*

- physics, 48, 330
- Halpern, J. P., Gotthelf, E. V., Leighly, K. M., & Helfand, D. J. 2001, *ApJ*, 547, 323
- Halpern, J. P., Camilo, F., Gotthelf, E. V., et al. 2001, *ApJL*, 552, L125
- Halpern, J. P., Gotthelf, E. V., Camilo, F., Helfand, D. J., & Ransom, S. M. 2004, *ApJ*, 612, 398
- Helder, E. A., Vink, J., Bamba, A., et al. 2013, *MNRAS*, 435, 910
- Henden, A. A., Templeton, M., Terrell, D., et al. 2016, *VizieR Online Data Catalog*, 2336,
- Hester, J. J. 2008, *ARA&A*, 46, 127
- Hillwig, T. C., & Gies, D. R. 2008, *ApJL*, 676, L37
- Hinton, J. A., Skilton, J. L., Funk, S., et al. 2009, *ApJL*, 690, L101
- Hobbs, G., Lyne, A. G., Kramer, M., Martin, C. E., & Jordan, C. 2004, *MNRAS*, 353, 1311
- Hobbs, G., Lorimer, D. R., Lyne, A. G., & Kramer, M. 2005, *MNRAS*, 360, 974
- Hoogerwerf, R., de Bruijne, J. H. J., & de Zeeuw, P. T. 2001, *AAP*, 365, 49
- Holland-Ashford, T., Lopez, L. A., Auchettl, K., Temim, T., & Ramirez-Ruiz, E. 2017, *ApJ*, 844, 84
- Horiuchi, S., & Beacom, J. F. 2010, *ApJ*, 723, 329
- Horiuchi, S., Beacom, J. F., Kochanek, C. S., et al. 2011, *ApJ*, 738, 154
- Huang, R. H. H., Wu, J. H. K., Hui, C. Y., et al. 2014, *ApJ*, 785, 118
- Hughes, J. P., Slane, P. O., Park, S., Roming, P. W. A., & Burrows, D. N. 2003, *ApJL*, 591, L139
- Hui, C. Y., & Becker, W. 2006, *AAP*, 454, 543
- Hui, C. Y., & Becker, W. 2009, *AAP*, 494, 1005
- Hui, C. Y., Seo, K. A., Lin, L. C. C., et al. 2015, *ApJ*, 799, 76
- Hulleman, F., van Kerkwijk, M. H., Verbunt, F. W. M., & Kulkarni, S. R. 2000, *AAP*, 358, 605
- Hulleman, F., Tennant, A. F., van Kerkwijk, M. H., et al. 2001, *ApJL*, 563, L49
- Iben, I., Jr., & Tutukov, A. V. 1996, *ApJ*, 456, 738
- Ihara, Y., Ozaki, J., Doi, M., et al. 2007, *PASJ*, 59, 811
- Jackson, M. S., Safi-Harb, S., Kothes, R., & Foster, T. 2008, *ApJ*, 674, 936
- Jennings, Z. G., Williams, B. F., Murphy, J. W., et al. 2012, *ApJ*, 761, 26
- Jiang, B., Chen, Y., & Wang, Q. D. 2007, *ApJ*, 670, 1142
- Johnston, S., Lyne, A. G., Manchester, R. N., et al. 1992, *MNRAS*, 255, 401
- Jones, S., Hirschi, R., Nomoto, K., et al. 2013, *ApJ*, 772, 150
- Kaplan, D. L., Frail, D. A., Gaensler, B. M., et al. 2004, *ApJS*, 153, 269
- Kaplan, D. L., Gaensler, B. M., Kulkarni, S. R., & Slane, P. O. 2006a, *ApJS*, 163, 344
- Kaplan, D. L., & Moon, D.-S. 2006b, *ApJ*, 644, 1056
- Kaplan, D. L., Chatterjee, S., Gaensler, B. M., & Anderson, J. 2008, *ApJ*, 677, 1201
- Kargaltsev, O., & Pavlov, G. G. 2007, *ApJ*, 670, 655
- Karpova, A., Zyuzin, D., Danilenko, A., & Shibanov, Y. 2016, *Journal of Physics Conference Series*, 769, 012002
- Kasliwal, M. M., Kulkarni, S. R., Gal-Yam, A., et al. 2012, *ApJ*, 755, 161
- Katsuda, S., Tsunemi, H., Mori, K., et al. 2012, *ApJL*, 754, L7
- Katsuda, S., Takiwaki, T., Tominaga, N., Moriya, T. J., & Nakamura, K. 2018, *ApJ*, 863, 127
- Keohane, J. W., Petre, R., Gotthelf, E. V., Ozaki, M., & Koyama, K. 1997, *ApJ*, 484, 350
- Kerzendorf, W. E., Do, T., de Mink, S. E., et al. 2018, *arXiv:1711.00055*
- Kobulnicky, H. A., & Fryer, C. L. 2007, *ApJ*, 670, 747
- Kobulnicky, H. A., Kiminki, D. C., Lundquist, M. J., et al. 2014, *ApJS*, 213, 34
- Kochanek, C. S. 2009, *ApJ*, 707, 1578
- Kochanek, C. S. 2017, *MNRAS*, 471, 3283
- Kochanek, C. S. 2018, *MNRAS*, 473, 1633
- Koo, B.-C., Yun, M.-S., Ho, P. T. P., & Lee, Y. 1993, *ApJ*, 417, 196
- Koo, B.-C., Lee, J.-J., Seward, F. D., & Moon, D.-S. 2005, *ApJ*, 633, 946
- Krause, O., Tanaka, M., Usuda, T., et al. 2008, *Nature*, 456, 617
- Kroupa, P., & Weidner, C. 2003, *ApJ*, 598, 1076
- Kulkarni, S. R., Clifton, T. C., Backer, D. C., Foster, R. S., & Fruchter, A. S. 1988, *Nature*, 331, 50
- Landecker, T. L., Roger, R. S., & Higgs, L. A. 1980, *A&AS*, 39, 133
- Large, M. I., Vaughan, A. E., & Mills, B. Y. 1968, *Nature*, 220, 340
- Leahy, D. A., & Ranasinghe, S. 2012, *MNRAS*, 423, 718
- Lin, L. C. C., Huang, R. H. H., Takata, J., et al. 2010, *ApJL*, 725, L1
- Liu, Z.-W., Tauris, T. M., Röpkke, F. K., et al. 2015, *AAP*, 584, A11
- Liu, Q. Z., van Paradijs, J., & van den Heuvel, E. P. J. 2006, *AAP*, 455, 1165
- Lockman, F. J., Blundell, K. M., & Goss, W. M. 2007, *MNRAS*, 381, 881
- Lopez, L. A., Ramirez-Ruiz, E., Huppenkothen, D., Badenes, C., & Pooley, D. A. 2011, *ApJ*, 732, 114
- Lorimer, D. R., Lyne, A. G., & Camilo, F. 1998, *AAP*, 331, 1002
- Lucas, P. W., Hoare, M. G., Longmore, A., et al. 2008, *MNRAS*, 391, 136
- Manchester, R. N., Hobbs, G. B., Teoh, A., & Hobbs, M. 2005, *AJ*, 129, 1993
- Margon, B. 1984, *ARA&A*, 22, 507
- Marshall, H. L., Canizares, C. R., Hillwig, T., et al. 2013, *ApJ*, 775, 75
- Martins, F., Schaerer, D., & Hillier, D. J. 2005, *AAP*, 436, 1049
- Matheson, H., Safi-Harb, S., & Kothes, R. 2013, *ApJ*, 774, 33
- Matsuura, M., Dwek, E., Barlow, M. J., et al. 2015, *ApJ*, 800, 50
- Maund, J. R., Smartt, S. J., Kudritzki, R. P., Podsiadlowski, P., & Gilmore, G. F. 2004, *Nature*, 427, 129
- Maund, J. R., Arcavi, I., Ergon, M., et al. 2015, *MNRAS*, 454, 2580
- Mavromatakis, F., Aschenbach, B., Boumis, P., & Papatastorakis, J. 2004, *AAP*, 415, 1051
- McGowan, K. E., Zane, S., Cropper, M., Vestrand, W. T., & Ho, C. 2006, *ApJ*, 639, 377
- Migliazzo, J. M., Gaensler, B. M., Backer, D. C., et al. 2002, *ApJL*, 567, L141

- Mignani, R. P., Perna, R., Rea, N., et al. 2007a, *AAP*, 471, 265
- Mignani, R. P., de Luca, A., Zaggia, S., et al. 2007b, *AAP*, 473, 883
- Mignani, R. P., de Luca, A., Mereghetti, S., & Caraveo, P. A. 2009, *AAP*, 500, 1211
- Mignani, R. P., Tiengo, A., & de Luca, A. 2012, *MNRAS*, 425, 2309
- Mignani, R. P., de Luca, A., Rea, N., et al. 2013, *MNRAS*, 430, 1354
- Miyaji, S., Nomoto, K., Yokoi, K., & Sugimoto, D. 1980, *PASJ*, 32, 303
- Moe, M., & Di Stefano, R. 2017, *ApJS*, 230, 15
- Moon, D.-S., Lee, J.-J., Eikenberry, S. S., et al. 2004, *ApJL*, 610, L33
- Moran, P., Mignani, R. P., Collins, S., et al. 2013, *MNRAS*, 436, 401
- Moritani, Y., Kawano, T., Chimasu, S., et al. 2018, *PASJ*
- Murray, S. S., Slane, P. O., Seward, F. D., Ransom, S. M., & Gaensler, B. M. 2002, *ApJ*, 568, 226
- Napoli, V. J., McSwain, M. V., Marsh Boyer, A. N., & Roettenbacher, R. M. 2011, *PASP*, 123, 1262
- Nasuti, F. P., Mignani, R., Caraveo, P. A., & Bignami, G. F. 1997, *AAP*, 323, 839
- Neckel, T., Klare, G., & Sarcander, M. 1980, *Bulletin d'Information du Centre de Donnees Stellaires*, 19, 61
- Ng, C.-Y., Romani, R. W., Briskin, W. F., Chatterjee, S., & Kramer, M. 2007, *ApJ*, 654, 487
- Ng, C.-Y., Kaspi, V. M., Ho, W. C. G., et al. 2012, *ApJ*, 761, 65
- Odegard, N. 1986, *ApJ*, 301, 813
- Paczynski, B. 1971, *ARA&A*, 9, 183
- Pannuti, T. G., Rho, J., Borkowski, K. J., & Cameron, P. B. 2010, *AJ*, 140, 1787
- Patel, S. K., Kouveliotou, C., Woods, P. M., et al. 2001, *ApJL*, 563, L45
- Patnaude, D. J., Lee, S.-H., Slane, P. O., et al. 2017, *ApJ*, 849, 109
- Pavlov, G. G., Zavlin, V. E., Sanwal, D., Burwitz, V., & Garmire, G. P. 2001, *ApJL*, 552, L129
- Pavlov, G. G., Sanwal, D., Kızıltan, B., & Garmire, G. P. 2001, *ApJL*, 559, L131
- Petre, R., Becker, C. M., & Winkler, P. F. 1996, *ApJL*, 465, L43
- Pineault, S., Landecker, T. L., Madore, B., & Gaumont-Guay, S. 1993, *AJ*, 105, 1060
- Ranasinghe, S., & Leahy, D. A. 2018, *AJ*, 155, 204
- Reed, J. E., Hester, J. J., Fabian, A. C., & Winkler, P. F. 1995, *ApJ*, 440, 706
- Reig, P. 2011, *Ap&SS*, 332, 1
- Remillard, R. A., & McClintock, J. E. 2006, *ARA&A*, 44, 49
- Renzo, M., Zapartas, E., de Mink, S. E., et al. 2018, *arXiv:1804.09164*
- Repetto, S., Igoshev, A. P., & Nelemans, G. 2017, *MNRAS*, 467, 298
- Reynolds, S. P., Borkowski, K. J., Hwang, U., et al. 2007, *ApJL*, 668, L135
- Reynoso, E. M., Green, A. J., Johnston, S., et al. 2004, *PASA*, 21, 82
- Reynoso, E. M., Cichowolski, S., & Walsh, A. J. 2017, *MNRAS*, 464, 3029
- Roberts, D. A., Goss, W. M., Kalberla, P. M. W., Herbstmeier, U., & Schwarz, U. J. 1993, *AAP*, 274, 427
- Romani, R. W., Ng, C.-Y., Dodson, R., & Briskin, W. 2005, *ApJ*, 631, 480
- Ruiz-Lapuente, P., Comeron, F., Méndez, J., et al. 2004, *Nature*, 431, 1069
- Safi-Harb, S., Ogelman, H., & Finley, J. P. 1995, *ApJ*, 439, 722
- Safi-Harb, S., Ribó, M., Butt, Y., et al. 2007, *ApJ*, 659, 407
- Salpeter, E. E. 1955, *ApJ*, 121, 161
- Sana, H., de Mink, S. E., de Koter, A., et al. 2012, *Science*, 337, 444
- Sandberg, A., & Sollerman, J. 2009, *AAP*, 504, 525
- Sarbadhicary, S. K., Badenes, C., Chomiuk, L., Caprioli, D., & Huizenga, D. 2017, *MNRAS*, 464, 2326
- Sasaki, M., Heinitz, C., Warth, G., & Pühlhofer, G. 2014, *AAP*, 563, A9
- Schaefer, B. E., & Pagnotta, A. 2012, *Nature*, 481, 164
- Schlafly, E. F., & Finkbeiner, D. P. 2011, *ApJ*, 737, 103
- Schwab, J., Quataert, E., & Bildsten, L. 2015, *MNRAS*, 453, 1910
- Schweizer, F., & Middleditch, J. 1980, *ApJ*, 241, 1039
- Seward, F. D., & Harnden, F. R., Jr. 1982, *ApJL*, 256, L45
- Shelton, R. L., Kuntz, K. D., & Petre, R. 2004, *ApJ*, 611, 906
- Skrutskie, M. F., Cutri, R. M., Stiening, R., et al. 2006, *AJ*, 131, 1163
- Slane, P., Seward, F. D., Bandiera, R., Torii, K., & Tsunemi, H. 1997, *ApJ*, 485, 221
- Slane, P., Zimmerman, E. R., Hughes, J. P., et al. 2004a, *ApJ*, 601, 1045
- Slane, P., Helfand, D. J., van der Swaluw, E., & Murray, S. S. 2004b, *ApJ*, 616, 403
- Slane, P., Hughes, J. P., Temim, T., et al. 2012, *ApJ*, 749, 131
- Staelin, D. H., & Reifenshtein, E. C., III 1968, *Science*, 162, 1481
- Strader, J., Chomiuk, L., Cheung, C. C., Salinas, R., & Peacock, M. 2015, *ApJL*, 813, L26
- Stupar, M., & Parker, Q. A. 2012, *MNRAS*, 419, 1413
- Swartz, D. A., Pavlov, G. G., Clarke, T., et al. 2015, *ApJ*, 808, 84
- Tam, C. R., Kaspi, V. M., van Kerkwijk, M. H., & Durant, M. 2004, *ApJL*, 617, L53
- Tananbaum, H. 1999, *CBET*, 7246, 1
- Tendulkar, S. P., Cameron, P. B., & Kulkarni, S. R. 2012, *ApJ*, 761, 76
- Tendulkar, S. P., Cameron, P. B., & Kulkarni, S. R. 2013, *ApJ*, 772, 31
- Tetzlaff, N., Neuhäuser, R., & Hohle, M. M. 2011, *MNRAS*, 410, 190
- Tian, W. W., & Leahy, D. A. 2013, *ApJL*, 769, L17
- Trepl, L., Hui, C. Y., Cheng, K. S., et al. 2010, *MNRAS*, 405, 1339
- Truelove, J. K., & McKee, C. F. 1999, *ApJS*, 120, 299
- Tuohy, I., & Garmire, G. 1980, *ApJL*, 239, L107
- van den Bergh, S. 1980, *Journal of Astrophysics and Astronomy*, 1, 67
- Verbiest, J. P. W., Weisberg, J. M., Chael, A. A., Lee, K. J., & Lorimer, D. R. 2012, *ApJ*, 755, 39
- Vink, J. 2012, *A&ARv*, 20, 49
- Waisberg, I. R., & Romani, R. W. 2015, *ApJ*, 805, 18

- Walter, R., Lutovinov, A. A., Bozzo, E., & Tsygankov, S. S. 2015, *A&ARv*, 23, 2
- Weisskopf, M. C., Swartz, D. A., Carramiñana, A., et al. 2006, *ApJ*, 652, 387
- Welsh, B. Y., & Sallmen, S. 2003, *AAP*, 408, 545
- Williams, B. J., Blair, W. P., Blondin, J. M., et al. 2011, *ApJ*, 741, 96
- Williams, B. J., Rangelov, B., Kargaltsev, O., & Pavlov, G. G. 2015, *ApJL*, 808, L19
- Willingale, R., Aschenbach, B., Griffiths, R. G., et al. 2001, *AAP*, 365, L212
- Winkler, P. F., Twelker, K., Reith, C. N., & Long, K. S. 2009, *ApJ*, 692, 1489
- Wolszczan, A., Cordes, J. M., & Dewey, R. J. 1991, *ApJL*, 372, L99
- Yamaguchi, H., Badenes, C., Petre, R., et al. 2014, *ApJL*, 785, L27
- Yatsu, Y., Kawai, N., Kataoka, J., et al. 2005, *ApJ*, 631, 312
- Yatsu, Y., Asano, K., Kawai, N., Yano, Y., & Nakamori, T. 2013, *ApJ*, 773, 25
- Zapartas, E., de Mink, S. E., Izzard, R. G., et al. 2017, *AAP*, 601, A29
- Zavlin, V. E., Pavlov, G. G., Sanwal, D., & Trümper, J. 2000, *ApJL*, 540, L25
- Zhao, H., Jiang, B., Gao, S., Li, J., & Sun, M. 2018, *ApJ*, 855, 12
- Zharikov, S. V., Shibanov, Y. A., Zyuzin, D. A., Mennickent, R. E., & Komarova, V. N. 2008, *AAP*, 492, 805
- Zharikov, S. V., Zyuzin, D. A., Shibanov, Y. A., & Mennickent, R. E. 2013, *AAP*, 554, A120
- Zhou, P., Vink, J., Li, G., & Domček, V. 2018, *ApJL*, 865, L6